上海交通大學

SHANGHAI JIAO TONG UNIVERSITY

学士学位论文

BACHELOR’S THESIS

论文题目：Fabrication and characterization of Li-ion based memristor synapse

学生姓名：李菲菲
学生学号：517021910887
专　　业：材料科学与工程（国际化试点班）
指导教师：吴蕴雯
学院(系)：材料科学与工程学院

上海交通大学

学位论文原创性声明

本人郑重声明：所呈交的学位论文《基于锂离子的忆阻器突触的制备与表征》，是本人在导师的指导下，独立进行研究工作所取得的成果。除文中已经注明引用的内容外，本论文不包含任何其他个人或集体已经发表或撰写过的作品成果。对本文的研究做出重要贡献的个人和集体，均已在文中以明确方式标明。本人完全意识到本声明的法律结果由本人承担。

学位论文作者签名：李菲菲

日期：2021 年 6 月 3 日

上海交通大学
学位论文版权使用授权书

本学位论文作者完全了解学校有关保留、使用学位论文的规定，同意学校保留并向国家有关部门或机构送交论文的复印件和电子版，允许论文被查阅和借阅。本人授权上海交通大学可以将本学位论文的全部或部分内容编入有关数据库进行检索，可以采用影印、缩印或扫描等复制手段保存和汇编本学位论文。

保密□，在___年解密后适用本授权书。

本学位论文属于

不保密☑。

（请在以上方框内打“√”）

学位论文作者签名：李菲菲　　　　指导教师签名：吴蕴雯

日期：2021年 6月 3日　　　　日期：2021年 6月 3日

锂离子型忆阻器突触的制备与表征

摘要

随着 21 世纪大数据时代的到来和集成电路领域的快速发展，计算机的整体计算能力受到了传统冯 • 诺伊曼结构的限制。忆阻器可以实现存算一体化，采用具有稳定阻变特性的新型忆阻器作为运算单元是突破冯 •诺伊曼瓶颈的一个有效途径。然而，忆阻器仍存在一些问题，包括工作电压较高、功耗较大和阻态数目较少等。锂离子型忆阻器主要通过锂离子在功能层的输运实现忆阻性能，为了解决上述问题，本研究主要从两方面展开研究：（1）采用纳米二氧化硅（SiO_2）掺杂的双三氟甲基磺酰亚胺锂-聚氧化乙烯（LiTFSI-PEO）固态电解质作为忆阻器的功能层薄膜，纳米颗粒的掺杂能够降低 PEO 膜的结晶度，从而调节离子电导率。基于此膜制得的 Au/Li-PEO-SiO_2/Si 忆阻器器件实现了较为稳定和对称的阻变（RS）性能与突触功能模拟。进行对比分析发现，纳米 SiO_2 对锂离子的吸附作用是实现对称 RS 特征的主要原因。与 Au/Li-PEO/Si 忆阻器相比，该忆阻器的工作功耗降低了 16.57%。（2）通过制备 Ag/Li-PEO/Si 忆阻器，结合银的电化学金属化（ECM）效应协同提高器件性能。该器件表现出稳定、多态的阻变（RS）特征，与 Ag/PEO/Si 忆阻器相比，工作功耗降低了 78.47%。本论文对锂离子型忆阻器的阻变现象及其机理的探索对未来离子型忆阻器的应用和发展具有一定的意义。

关键词：锂离子，忆阻器，固态电解质，阻变特征

FABRICATION AND CHARACTERIZATION OF LI-ION BASED MEMRISTIVE SYNAPSE

ABSTRACT

With the advent of the era of big data in the 21st century and the rapid development of integrated circuit, the overall computing power of computers has been limited by the traditional von Neumann structure. Memristor can realize the integration of memory and computation, thus it is an effective way to break through the Von Neumann bottleneck by using novel memristor with stable resistance switching (RS) property as the computing unit. However, there are still some problems with memristors, including high working voltage, large power consumption and few resistance states. Lithium-ion based memristor mainly realizes RS through the transport of Li ions in the function layer. Therefore, to solve the problems above, this work is mainly carried out from two aspects: (1) nano-SiO_2 doped lithium bis trifluoromethyl sulfimide-polyvinyl oxide (LiTFSi-PEO) solid electrolyte was used as the function layer of the memristor. The doping of nanoparticles can reduce the crystallinity of the PEO film, so as to modulate the ionic conductivity. The Au/Li-PEO-SiO_2/Si memristor device based on this membrane has achieved stable and symmetrical RS performance and simulation of synaptic function. Through analysis, it is found that the adsorption of Li ions by nano-SiO_2 is the main reason for achieving the symmetrical RS property. Compared with Au/Li-PEO/Si memristor, the working power consumption of the memristor is reduced by 16.57%. (2) By fabricating Ag/Li-PEO/Si memristor and combining with the electrochemical metallization (ECM) effect of silver, the device performance was improved. Compared with Ag/PEO/Si memristor, the device exhibits a stable and multi-level RS properties, and the working power consumption is reduced by 78.47%. The exploration of the RS phenomenon and mechanism of Li-ion based memristor is of certain significance to the application and development of ionic memristor in the future.

Key words: Lithium ion, Memristor, Solid electrolyte, RS properties

Contents

Chapter 1 Introduction and Background

1.1 Introduction

With the arrival of big data age in the 21st century and the rapid development in the field of integrated circuits, Moore's Law has reached its physical limit. To meet the development of intelligence and interconnection, higher and higher requirements are putting forward for memory capacity, calculation rate and consumption of computer. Although at present some memory and processor can reach high speed, traditional computers are limited by the von Neumann architecture with the data stored in memory and transported to the calculating cell. Thus restrict the overall computing capacity, which is commonly known as the "memory wall".

To solve von Neumann bottleneck, there are two main directions. One is to reduce the cost of data movement between the computation cell and the memory by increasing the storage capacity and making it closer to the calculation cell. The other is to realize the computation directly in the memory cell, which can reduce the energy consumption of data transmission and improve the efficiency. Therefore, the integration of data storage and computation is an important research subject under the background of the current era.

Inspired by human's brain and nervous system, neuromorphic computing is an emerging way to break von Neumann's limitation. Brain, as the information processing center, can implement advanced computing tasks such as learning, memory, recognition and perception with highly integration (the volume of brain is about 1.2 L) and low energy consumption (about 20 W)[1]. The superiority of brain includes highly parallel at single node, low-energy processing[2], high fault-tolerance, and learning ability according to the external environment, etc. These all depend on the enormous connection between the cerebral cortex neuron network while synapses are the important structure for information transmission. Synaptic plasticity underlies brain functions such as learning and memory[3]. Therefore, the limitation of the traditional von Neumann architecture can be overcome through artificial synapses, which have been proved to have broad application prospects in artificial neural networks[4], backpropagation simulation[5] and other fields.

Current novel artificial synapse devices include memristors, phase change memory[6] and field effect transistors[7]. Due to the simple structure and preparation, good scalability, considerable integration[8], high compatibility with CMOS circuit and other advantages, memristors gain increasing researching interest. The study of the memristors is under rapid development and prepare advanced materials with better stability and performance for memristors is the focus of research in material science, physics and other field of discipline.

1.2 Memristor

1.2.1 History of memristor

Memristor, which means memory and resistance, is the fourth kind of basic circuit elements beyond resistance, capacitance and inductance. In 1971, Pro. Chua proposed the concept of memristor for the first time[9] based on the symmetry in physics. However, the memristor remained in the theoretical stage for several decades after it was proposed. Until 2008, the existence of memristor was firstly confirmed when HP Laboratory first realized the solid memristor based on titanium dioxide film[10], which set off a research boom in memristor. The emergence of memristor devices is expected to realize non-volatile random access memory. Moreover, the integration, power consumption, and reading and writing speed of the memristor-based random access memory are all superior to the traditional random access memory. In addition, memristor is one of the best choices to implement artificial neural network synapses on hardware. With the non-linear nature, memristor can generate chaotic circuits, which also have many applications in secure communication. Thus, the research of memristors become hotpot then.

1.2.2 Basic concepts of memristor

Memristor is an electronic component that expresses the relationship between magnetic flux and electric charge. It has the dimension of resistance, but unlike resistance, the resistance of memristor is determined by the amount of historical charge flowing through it, and can maintain this resistance value after removal of power, that is, it is non-volatile. Therefore, by measuring the resistance of the memristor, the amount of charge flowing through it can be calculated, and thus have the function of memory charge, or memory resistance.

DC current-voltage (I-V) sweeping is one kind of important characterization method to measure the electric performance of memristors. SET and RESET are two common behaviors for memristor devices. The former one means that the device changes from high resistance state (HRS) to low resistance state (LRS), while the later one means the reverse change, from LRS to HRS. Lower SET and RESET voltage means lower power consumption and easiness to regulate the devices. Another important concept of I-V properties is the ON/OFF ratio, which can be valued by the formula below:

$$ratio = \frac{G_{LRS}}{G_{HRS}} = \frac{R_{HRS}}{R_{LRS}} \qquad (1-1)$$

Where G_{LRS} and G_{HRS} represent the conductance value at LRS and HRS and R_{LRS} and R_{HRS} represent the resistance value at LRS and HRS. Higher ON/OFF ratio can provide distinct resistance levels, which is beneficial to the recognition of different resistance states and the storage of the data in devices.

In DC I-V sweeping, a continuously varying voltage is applied to one electrode, and there shows four types of the I-V characteristics as drawn in Fig. 1.1[11]. Write-once-read-many (WORM) shows one SET behavior and remains the low resistance state (Fig. 1.1a), useful for important data storage. The resistance switching behaviors (SET and RESET) of bipolar type device depend on the polarity of the bias applying, that’s SET at one bias and RESET at opposite bias (Fig. 1.1b). Both bipolar- and unipolar-type can be used in repeatable write-wipe memory. While for unipolar type (Fig. 1.1e), it only depends on the amplitude of applied voltage. The memrisive type (Fig. 1.1d) with consecutive modulation of resistance or conductance, which is similar to the memory pattern in human brain, is novel for simulating the neural network. By analyzing the I-V characteristic of the memristor devices, we can get a further insight of the mechanism and application of RS behaviors. One application is the artificial synapse. The electrical properties of memristors have similarities with synaptic functions or synaptic plasticity. For example, in a unipolar I-V sweeping cycle, the continuous increase or decrease in the output current of the device is similar to the excitation and inhibition functions of the synapse during the signal afferent process[12]. Therefore, it is common to use memristor devices to simulate synaptic behavior and further apply in neutral network computing.

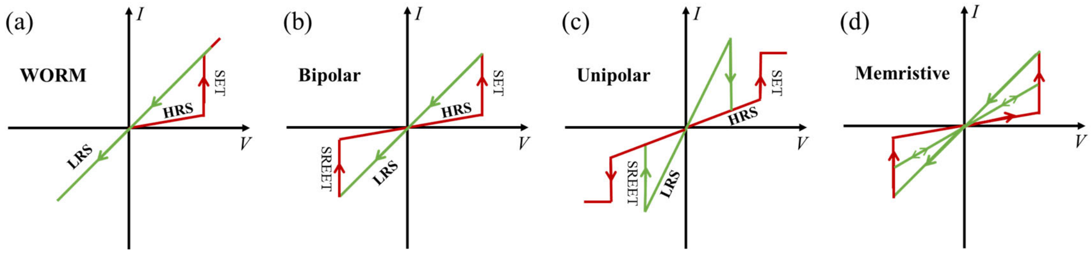

Fig. 1.1 Schematic of 4 varies I-V characteristics of resistive switching memories[11]

1.2.3 Types and mechanisms of memristor

As one important advantage, memristor has simple structure. It is mainly a sandwich structure composed of top electrode, medium function layer and bottom electrode. This device structure enables high-density data storage by integrating in vertical and three-dimensional crossbar array[13].

According to the medium function layer materials, memristors can be divided into several types. The function layer is pivotal as it will change its resistance value according to the applied voltage and its own material characteristics, so as to achieve the effect of “resistor-memory”. There are many kinds of materials used as the medium layer, such as inorganic oxide (ITO[14], Al_2O_3[15, 16], TiO_2[16, 17]), two-dimensional materials (MoS_x[16, 18], graphene and its oxides [16, 17], hexagonal boron nitride[19]), and polymer (polyvinylpyrrolidone[20], polyvinyl alcohol[21], poly oxyethylene[22]) with certain conductivity.

There are three main working mechanisms of memristor: conformational-changing-[23], ferroelectric-[24] and ionic-type, showing different I-V properties as illustrated in Fig. 1.2. The resistance changing of the ionic-type ones is mainly caused by the ions transport and chemical reaction under the external electric field, which includes anion (mainly oxygen ions) effect and cationic (mainly electrochemically active metal ions, such as Ag^+, Cu^{2+}, etc.) effect[25].

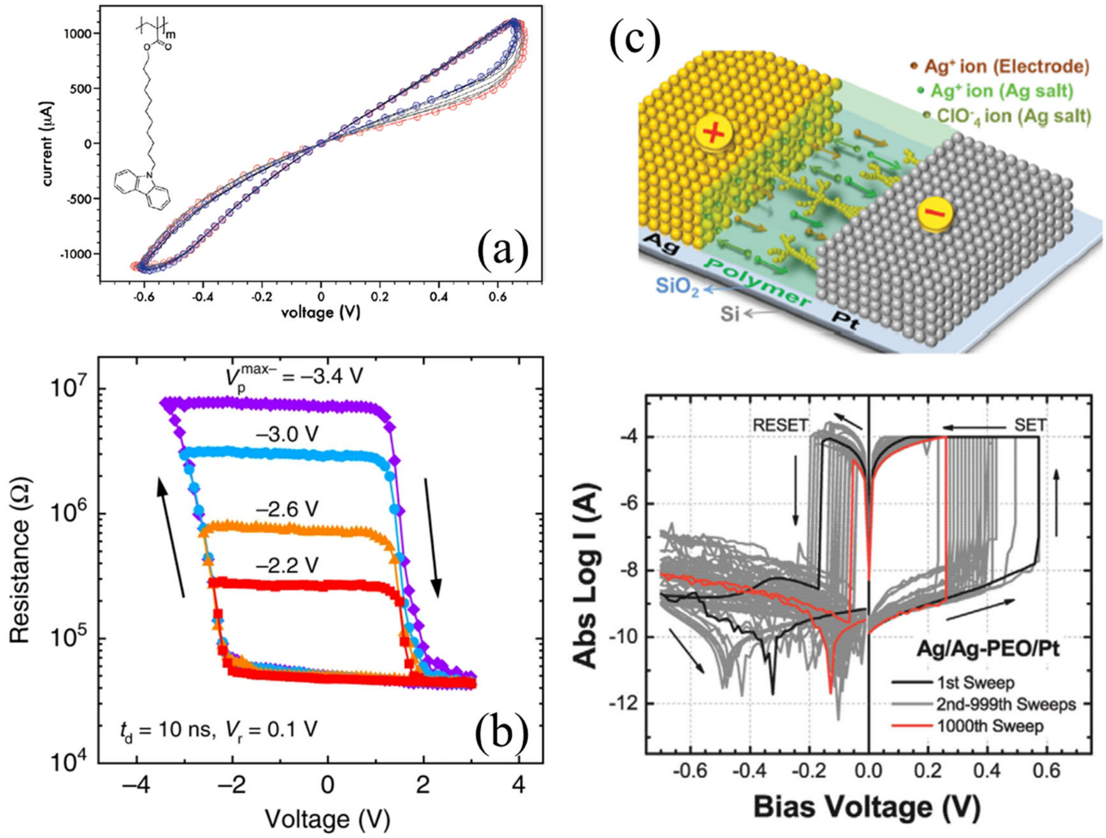

Fig. 1.2 Three main working mechanisms of memristor: (a) conformational-changing-[23], (b) ferroelectric-[24] and (c) ionic-type[26]. The upper one of (c) is the structure and the lower one is the I-V sweeping

The cationic effect is also called the electrochemical metallization (ECM)[27] cell, with the feature of formation and fracture of conductive filaments (CFs). In this way, the electrode contributes to the RS behaviors as well as the medium function layer. The area of electrodes does not affect the change of resistance with the assumption of the random formation of the CFs. A typical trait of ECM devices is the need for an electrochemically active metal electrode, such as Ag, Cu, or alloy containing an active metal. And the other electrode is generally electrochemical inert, such as Pt, Au, etc. The resistance changing effect of this kind of devices are based on the physical migration and electrochemical reaction of the active metal ions in the solid electrolyte. When a positive bias applies on the active electrodes, the metal ions will transfer to the inert electrode and be reduced into metal atoms, finally forming a metal filament connecting the two electrodes as the conductive path, as shown in Fig. 1.3. The conductive filament lowers the resistance of the devices significantly, thus changing the resistance states. This is the “write” process. “wipe” the devices is similar to “write”, in which a negative bias applies on the active electrode and forces the metal ions go back from the filaments to the active electrode, thus broking the filaments and returning to high resistance state[25]. By controlling the amplitude and width of the voltage applying on the electrode, the thickness of conductive filaments and the irreversible connection can be adjusted, so that the weight of synapses can be reflected by the various conductance states, and the short-term and long-term synaptic plasticity can be realized[20].

During the I-V sweeping of ECM devices, there are two kind of SET voltage: “forming” at the first cycle and “switching” in the following cycles[27], as **Fig. 1.3**(a) shows[28]. Usually, the forming voltage is higher than the switching voltage since the nano-channel formed during the 1st cycle may remain after the 1st reset and provide an inner surface available for the subsequent growth of conductive filaments.

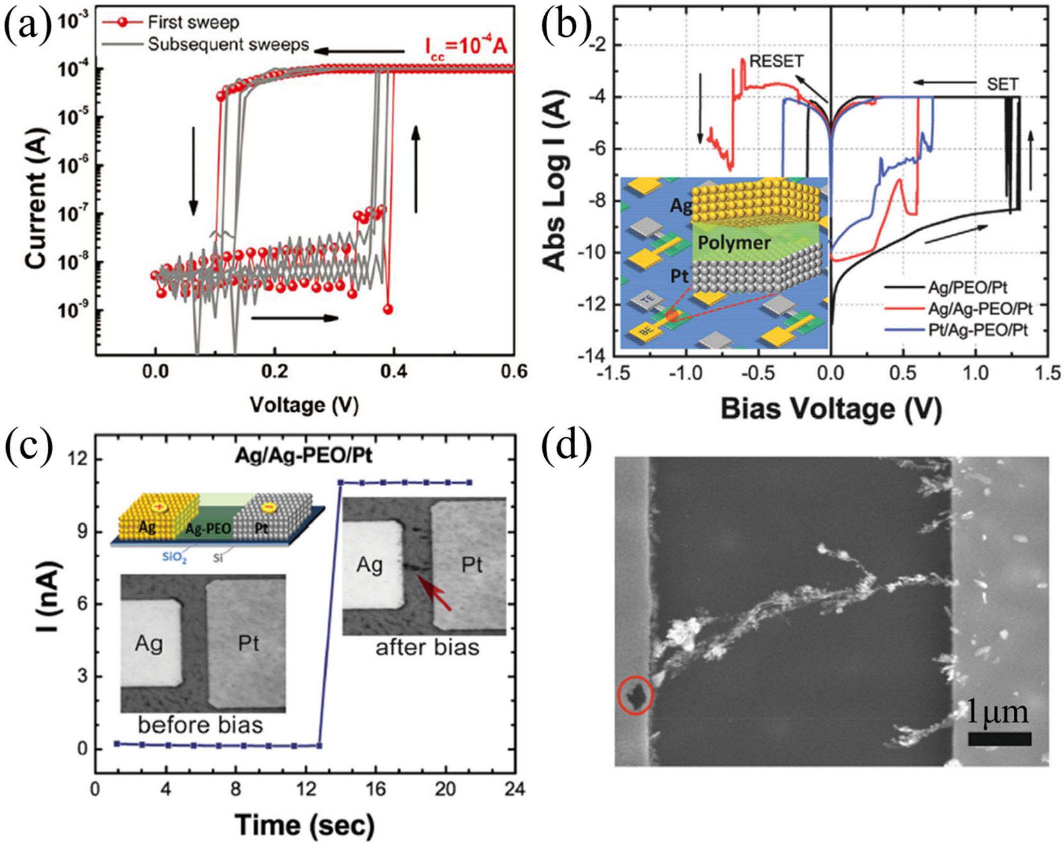

Fig. 1.3 ECM memristor device. (a): Forming and switching voltage[28]. (b): I-V sweeping for Ag/polymer/Pt ECM device. (c) and (d): Formation and dissolution of Ag CFs[26]

Among different kinds of medium layer materials, lithium as the main conductive ions is the promising one and the Li-ion based memristor typically belongs to ionic-type.

1.3 Lithium-ion based memristors

Lithium metal has the lowest electrochemical potential (-3.04 V vs standard hydrogen electrode), high reactivity[29], small ionic radius and large diffusion coefficient. With the accelerating requirement of power density, lithium become the most popular material for the application of rechargeable energy storage and other fields.

1.3.1 Li-PEO solid electrolyte

Metal ions are common-used conductive materials, and lithium salt is widely used as solid electrolyte material for lithium batteries, known as lithium ion batteries (LIBs). Compared with their common liquid counterparts, solid polymer electrolyte (SPE) solves the safety issue and has better flexibility and processability, thus becoming a promising electrolyte material. Not only can reduce the flammability and possible side reactions with the electrode, SPE also retain the excellent adhesion and film-forming properties of the polymer. In addition, the solid electrolyte membrane can also inhibit the growth of lithium dendrites, thereby further ensuring the safety of the battery during charging and discharging. In 1973, Fenton et al.[30] reported that ions migration in polyoxyethylene (PEO)-alkali metal salt complexation, which writes a new chapter in the research of SPEs. Later in 1979, Armand et al.[31] reported that the ionic conductivity of this complex can reach as high as 10^{-5} S/cm, indicating that SPE cans be used at room temperature, broaden the application scope.

PEO-Li salt compound is a mature and widely used electrolyte for LIBs. Many Li salts are used in PEO-Li system, such as lithium perchlorate ($LiClO_4$)[32, 33], lithium tetrafluoroborate ($LiBF_4$)[34] and lithium hexafluorophosphate ($LiPF_6$)[34]. For most Li-ion SPE, the ionic conductivity is about 10^{-5} S/cm at room temperature[34, 35] and higher (10^{-4} S/cm)[34] at high temperature. The lithium transference number is about 0.1~0.3[35, 36].

Among the commonly used Li salts, Bis(trifluoromethane)sulfonimide lithium salt (LiTFSI) has been intensively studied as the main salt of solid electrolyte among a variety of lithium salts in recent years, which is already used in electric vehicles[36]. There are some intrinsic advantages of LiTFSI[36], including the high flexibility of -

SO2-N-SO2- segment, high delocational charge distribution which can enable good Li+ movement due to the reduced interaction between Li+ and TFSI-, good thermal, chemical and electrochemical stability, outstanding solubility and highest conductivity, etc.

The lithium ions transport among the PEO segment in electrolyte layer. Due to the existence of the strong electron-donating ether group (-O-) and polar group, PEO can bind to the cation of various metal salt even at very high concentration, making the ion migration faster. PEO is also chemically and electrochemically stable with C-H, C-C and C-O bonds in its structure (Fig. 1.4a). When compounded LiTFSI with PEO, the weak interaction between Li+ cation and TFSI- anion makes Li+ easy to be trapped within PEO chains[37], while the anions are fixed to the macromolecular skeleton by covalent bonds. With proper doped concentration, the flexible TFSI- anion reduces the crystallinity. It's generally accepted that both the intrachain and interchain transport of Li+ ions in PEO depends on the segment motion of the polymer backbone in the amorphous phase[34] (Fig. 1.4c and d). Thus, the crystalline regions functions as obstacle for ion transport in PEO, explaining that the addition of LiTFSI can enhance the ion motion across the electrolyte.

To further improve the conductivity of Li-PEO at ambient temperature (10^{-6}~10^{-9} $S\cdot cm^{-1}$), there are generally three effective strategies, that's making (1) polymer/liquid hybrid, (2) polymer/polymer hybrid[38] and (3) polymer/ceramic hybrid. Doping ceramic nanofillers, such as ceramic fillers[39, 40] and silica oxide nanoparticles[41, 42] can enlarge the amorphous area of the Li-PEO electrolyte, in other word, lower the crystallinity. Since the Li ion mainly transports among the amorphous region of the polymer[34], lower crystallinity is beneficial to the Li ion movement. At the same time, addition of inorganic fillers can change the local Li^+ environment to activate more mobile Li^+ in the polymer. Owing to the surface interactions between the polymer electrolytes with molten lithium and inorganic fillers, more surface defects of fillers are generated, consequently improving the polymer/lithium interaction, local environment of Li^+ and activation energy of Li^+ transmission.

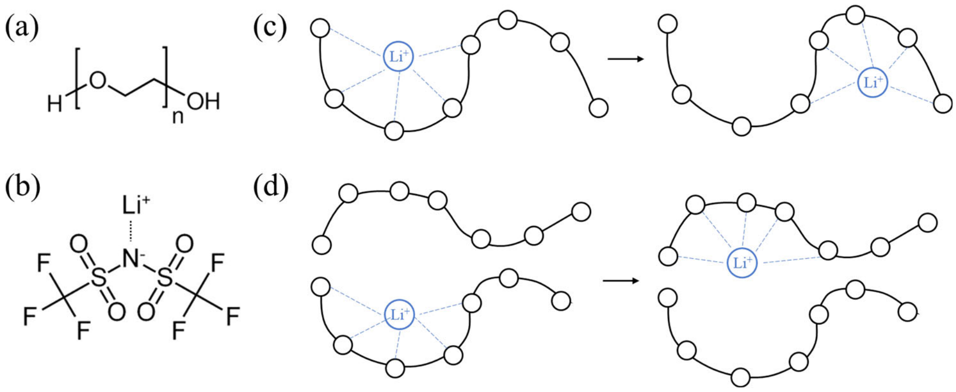

Fig. 1.4 Schematic of (a) PEO structure, (b) LiTFSI structure and (c) intrachain and (d) interchain transport of Li ion in PEO

Surface-modification of SiO_2 with silane coupling agent[43, 44] or using novel SiO_2 morphology[45, 46] are also commonly used to make SiO_2 more miscible in polymer, as well as to improve the mechanical property or flexibility.

1.3.2 Materials of Li-ion based memristor

Beyond the energy storage, the Li-ion electrolytes or conductors can offer other numerous functions beyond energy storage in thin-film form[47], including in-memory computing, artificial synaptic plasticity, and smart sensing. Consider the features mentioned above, memristor with Li^+ as movable conductive ions may achieve some great properties like good ionic conductivity, long life, high energy density, environment friendly, etc. Owing to the excellent properties of Li-ion electrolyte, researchers begin to use it as the function layer of memristor.

Li-ion based memristor has fast response speed, and can achieve lower power consumption. This kind of memristors has realized some basic properties of resistance or conductance modulation and synaptic plasticity functions.

A lot of Li salts successfully realize the memristor function. Common Li salts include $LiNbO_3$[48-50], $LiClO_4$[51], Li_2CO_3[52], $LiCoO_2$[4, 53] and $LiNO_3$[13]. These Li memristors can achieve stable SET and RESET behavior (Fig. 1.5a), multi-level conductance states (>250 in Fig. 1.5b). Both short-term plasticity (STP) and long-term plasticity (LTP) (Fig. 1.5b) and the STP-to-LTP transition[51] of synaptic can be stimulated by Li-ion based memristors, such as excitatory postsynaptic current (EPSC)[51, 54], paired-pulse facilitation (PPF)[54], spike-rate dependent plasticity (SRDP)[2, 54], etc. They can also simulates some advanced learning and cognitive functions, such as associative learning (Pavlov dog experiment)[54] and experiential learning[55]. Use Li-ion based memristor in neuromorphic network like image recognition, the recognition accuracy can reach as high as more than 90%[5, 56].

Sometimes more than one kind of Li salt will be used, like $LiCoO_2$ + LiPON[57], where LiPON acts as Li supplement and buffer layer. With LiPON layer, memristor shows better retention since this layer can prevent Li ion from self-injection, as demonstrated in Fig. 1.5(c) and (d).

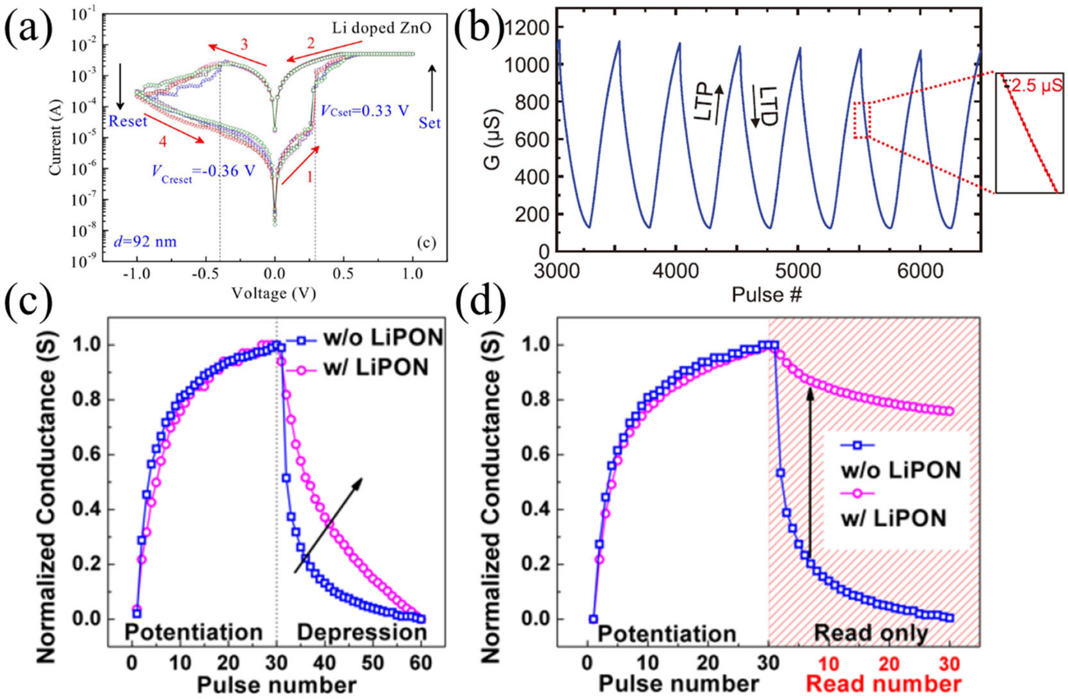

Fig. 1.5 (a) Stable RS behavior of Li_2CO_3[52]. (b) >250 conductance states of

$LiCoO_2$[53]. (c) and (d) improved retention with two Li salt $LiCoO_2$ + LiPON[57]

Doping Li with SiO_2[58] or TiO_2[2] is another way to prepare the memristor function layer. Wu et al. [58] deposited 5nm Li_xSiO_y by magnetron sputtering as the function layer and the device demonstrated obvious SET and RESET behavior with compliance current of 100 μ A. $LiSiO_X$ memristor[56] realizes stable RS property as well as the good spatial (device-to-device) stability for long-term plasticity as shown in Fig. 1.6, which is of great significance to the practical application of the device.

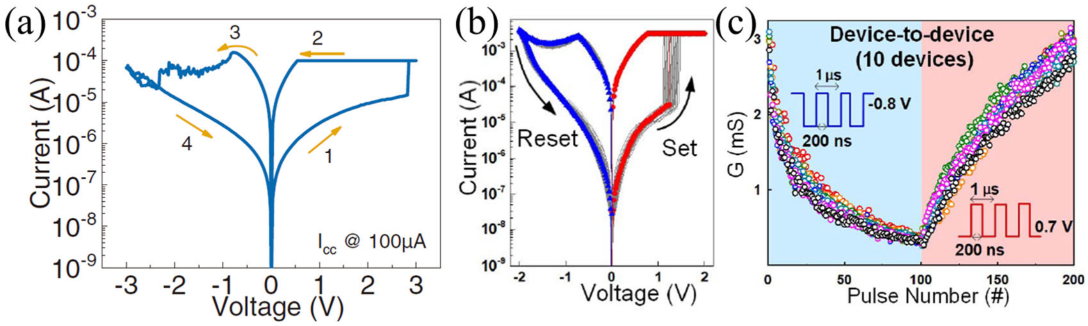

Fig. 1.6 Electric property of Li-Si. (a) RS property of Li_xSiO_y[58]. (b) stable RS and spatial stability of $LiSiO_X$[56]

1.3.3 Working mechanism of Li-ion based memristor

The resistance changing mechanism of Li-ion based memristors can be mainly divided into three types below.

(1) Intercalation and deintercalation of Li ions, also called alloying effect of Li. Li ions can react with various materials, like graphene[53], amorphous Si[4], SnO_2[51] and LiPON[57]. With applied electric bias, the Li ions move toward bottom electrode and intercalate into the Li "storage" layer, usually increase the conductivity. Then with opposite bias, the Li ions can be deintercalation, lowering the conductivity again, as illustrated in Fig. 1.7. Li can also react with ZnO, alloying with Zn into Li-Zn pairs with lower Gibbs free energy[13] at the Li-ZnO/ZnO interface after Li ions migrated and

aggregated near the interface.

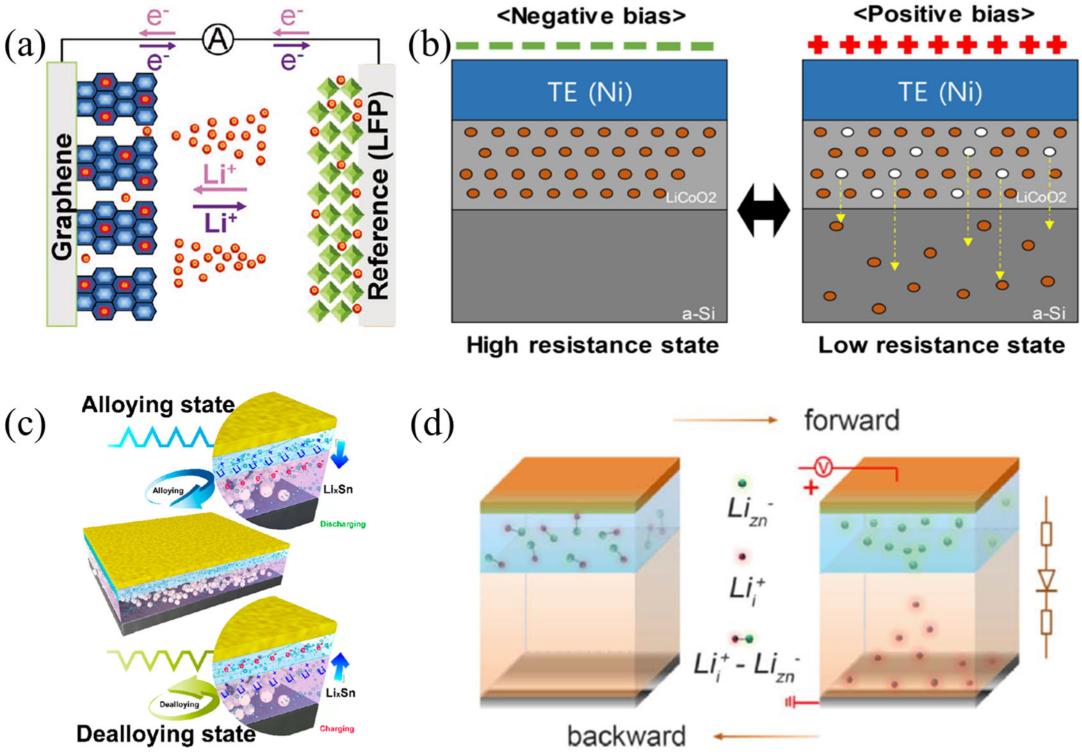

Fig. 1.7 Intercalation and deintercalation of Li in (a) graphene, (b) amorphous Si, (c) SnO$_2$ and (d) ZnO layer

(2) Combined movement of Li movement and oxygen vacancies. Li movement will affect the content and position of oxygen vacancies, thereby regulating the resistance value[48, 56]. When applying bias with unchanged polarity, Li ions and oxygen vacancies can accumulate and continuously enhance the conductance, as Fig. 1.8(b) shows.

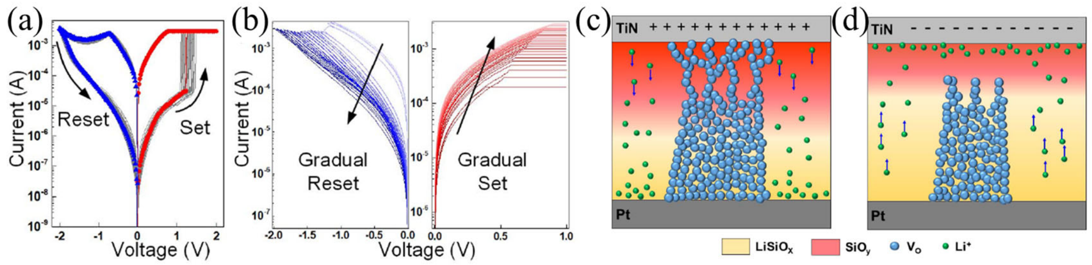

Fig. 1.8 Li movement and oxygen vacancies[56]. (a) I-V sweeping, (b) unipolar I-V sweeping and schematic of RS mechanism with positive (c) and negative (d) bias

(3) Formation and dissolution of Li-containing phases. Wu et al. found that for TiN/Li_xSiO_y/Pt[58], the formation and dissolution of crystalline lithium titanium silicate ($LiTiSiO_4$) phase confirmed by line scan EDS spectrum and HRTEM image change the conductivity of the memristor. With external bias, the Li forms conductive $LiTiSiO_4$ connecting two electrodes, thus displaying RS behavior. Li can also migrate to interstitial and substitutional position of ceramic lattice structures[52], thus changing the crystallinity of each phase and then the conductivity. The formation and dissolution process are illustrated in Fig. 1.9.

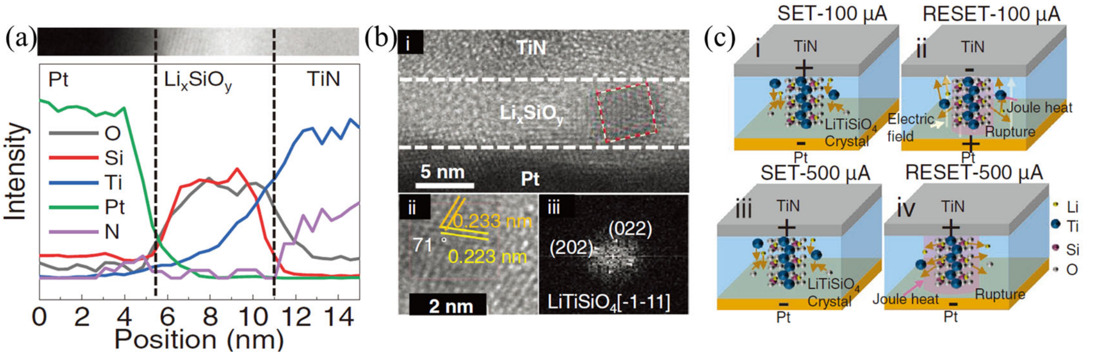

Fig. 1.9 Formation and dissolution of Li-containing phase[58]. (a) line scan EDS spectrum and (b) HRTEM image of $LiTiSiO_4$. (c) schematic of RS behavior

Other RS mechanism include the shift of Li ions[48, 50], electrochemical reaction of non-Li ions (for example, Co^{3+} to Co^{4+} from $LiCoO_2$) within function layer[2] and Joule heat[58, 59].

However, for most Li-ion based memristor, the resistance changing mechanism is more complex, since there may be more than one RS mechanism. Therefore, various methods should be used to analyze the RS mechanism according to the actual situation.

1.3.4 The prospect of Li-ion based memristor

Li-ion based memristor artificial synapses have broad application prospects [25], for example: 1) high-density information storage. The memristor's multi-resistance state can be used for multi-value storage. With cross-bar structure, memristors are stacked in three dimensions, and by further downscaling the device to atomic size, storing information at a very high density; 2) Logical operation. The memristor breaks the von Neumann bottleneck and can simultaneously perform data storage and Boolean logic operations. It can be used as a data processor as well; 3) Neural network simulation. Memory characteristic of memristors is similar to synaptic plasticity. Compared that the synapses adjust the information transmission capacity through the release of Ca^{2+} and Na^{+} ions, the process of memristors is done by transportation of oxygens ion or metal ions, which can be accurately controlled through the regulation of the external environment. Some researchers also combined the memristor with other modules to realize sensing and other functions like visual storage system[60].

1.4 Significance and research content of this thesis

Some problems still exist for Li-ion based memristor at present, such as high programming power, poor performance stability, and nonlinear characteristics[57]. Also, the resistance changing mechanism remains unclear, inhibiting the practical applications of Li-ion based memristors. And the commonly used electrolyte system, LiTFSI-PEO, also confront some challenges: it’s hard for LiTFSI to dissolve completely, leading to some undesired cluster[61]. The solid polymer membrane also has the same problems as the SPEs, such as huge interfacial resistance and low bulk conductivity at room temperature, which is unfavorable for ion transport.

Considering the excellent electrical conductivity and fast response speed of Li-ions as well as the merits of SPE, this work intends to prepare Li-PEO solid electrolyte as the function layer and fabricate Li-ion based memristors. To solve the problem of excessive power consumption, we intended to add nano SiO_2 into the function layer. Also, to combine the ECM and the Li migration, we used active Ag as top electrode to structure the Li-ion memristor. The main contents of this work are shown below.

In chapter 3, we prepared Li-20PEO electrolyte membrane by multi-step spin-coating method. We adjusted the preparation process and obtained ideal thickness and roughness. The membrane was characterized with several kinds of characterization methods, including SEM, EDS, AFM, XRD and EIS. Then we added nano SiO_2 particle into the electrolyte to observe the influence of SiO_2 on the surface quality, crystallinity and ionic conductivity. Finally, Au/Li-PEO/Si and Au/Li-PEO-SiO_2/Si memristor devices were fabricated. To preliminarily explore the electrical performance and basic resistance changing properties, DC current-voltage (I-V) sweeping was conducted. Based on the I-V curves, the power consumption was calculated and some resistance changing mechanism were put forward.

In chapter 4, Ag was used as top electrode to combine the ECM and Li ion transport. The DC I-V sweeping of Ag/PEO/Si and Ag/Li-PEO/Si were measured and the I-V properties were analyzed. To exclude the influence of naturally grown SiO_2 on Si, Ag/PEO/ITO was fabricated. We characterized the surface flatness of PEO/ITO by SEM and tested its I-V properties within different voltage range. By analyzing the I-V curves, the power consumption was calculated and some resistance changing mechanism were arisen.

This work adds a new choice to the fabrication of memristors by applying the common LiTFSI-PEO battery system to memristor. The study of I-V property and the resistance changing mechanism model raised are significant to the future research and helpful to broaden the application filed. This work also provides new ideas to decrease the power consumption as well as overcome the stability problem, which is of certain significance to the application and development of ionic memristor in the future.

Chapter 2 Fabrication, characterization, and analysis methods

2.1 Material and equipment

2.1.1 Reagent and material

The chemical reagents used in the experiment are listed in Table 2.1.

Table 2.1 Chemical reagent

Name	Chemical formula	Purity and specification	Manufacturer
Polyoxyethylene (PEO)	$H(C_2H_4O)_nOH$	Average Mv ~300,00 powder	Sigma-aldrich
Lithium bis (trifluoromethulfonyl) imide (LiTFSI)	$C_2F_6LiNO_4S_2$	98% +	Shanghai Titan Scientific Co., Ltd
Nano SiO_2 particles	SiO_2	Average diameter ~10nm	China
Acetonitrile (ACN)	C2H3N	99.8%, anhydrous, H_2O: ≤0.005%	Aladdin
Acetone	CH3COCH3	AR	Sinopharm Chemical Reagent Co., Ltd
Ethanol	C2H5OH	AR, anhydrous, ≥99.7%	Shanghai Titan Scientific Co., Ltd
Single polished silicon wafer	Si	P<100>	Lijing Optoelectronic Technology
Indium Tin Oxide (ITO)	In2O3-SnO2	OPV-ITO 11-7	OPV Tech New Energy Co., Ltd

2.1.2 Equipment

The instruments and equipment used in the experiment are listed in Table 2.2.

Table 2.2 Instruments and manufacturers

Instrument Name	Model	Manufacturer country or company
Glove box	SMART (1200/750)	Eminex Science & Technology (Beijing) Co., Ltd
Magnetic stirrers	SN-MS-M2	Shangpu Co., Ltd
Spin coater	EZ4	LEBO science Instrument Co., Ltd
Simple hot plate	HP10	LEBO science Instrument Co., Ltd
High vacuum resistance evaporation coating equipment	VZZ-300	Vnano Vacuum Technology Co., Ltd.
UV surface irradiation device	BZZ250G-T	Huiwo Technology Co., Ltd
Ultrasonic cleaner	SK2200H	Shanghai Kudos Ultrasonic Instrument Co., Ltd
Electronic scales	FC-50	Shenzhen Aweigh Electronic Co., Ltd.
Constant temperature heating plate	Kaisi 818	UYUE
Hydraulic Crimper	MSK110	MTI corporation
Keithley Semiconductor Parameter Analyzer	4200A-SCS and 2400 SMU	Keithley Instruments, Inc.
Electrochemical workstation	CHI660E	Shanghai Chenhua Instrument Co., Ltd
X-ray diffractometer	Ultima IV	Japan

Table 2.2

Instrument Name	Model	Manufacturer country or company
Scanning electron microscope	Mira3 LHM	Oxford Instruments
Surface profilometer	Alpha-step D-600	America
Atomic force microscope	MFP-3D	Oxford Instruments

2.2 Fabrication method of Li-PEO electrolyte film

The Li-polymer electrolyte films were prepared by spin-coating method for memristor devices and solution casting method for other characterizations and measurements.

2.2.1 Spin-coating method

Spin-coating is a coating process in which the droplets on the workpiece are fully distributed on the surface of the workpiece by the centrifugal force and gravity when the workpiece is rotating. Spin-coating is only suitable for the preparation of one-sided coating on simple planar workpiece, mainly used for the preparation of electron beam tube fluorescent screen coating, etc. The main advantages of spin-coating include: easy to obtain a higher density coating film, and the coating thickness is uniform. The thickness of the membrane is proportional to the second power of the solution viscosity, and inversely proportional to the square root of the rotating speed.

In the experiment, the membrane on the device was prepared by spin-coating method. After cleaning the substrate and preparing the solution, drop several drops of the prepared solution to the substrate and spin-coated with the coater at ambient temperature. The schematic of the spin-coating process is shown in Fig. 2.1(a).

2.2.2 Solution casting method

For some characterization like XRD, the thickness of the films should be not too small. So that use the solution casting method to gain thicker film. This is also a common way to get electrolyte film in battery. During solution casting, solutions and solvents are poured into molds and the solvents evaporate gradually. It generally does not apply pressure, having low demand to the apparatus. The polymer, in fact, must be soluble in the selected solvent in an appropriate concentration which is strictly related to final membrane application.

The substrate cleaning and the solution preparation was the same as the spin-coating method. The solution was then cast on a polytetrafluoroethylene mode covered with a layer of silicone paper (to make it easier to peel off) and dry at ambient temperature for more than 48 hours. Peeled off the dried film and it can be punched into circular pieces for subsequent characterizations or measurements.

2.3 Fabrication of devices

2.3.1 Substrate cleaning

The p-type doped silicon with high conductivity was selected. The silicon wafer (with resistivity 0.01 ~ 0.02 Ω·cm and thickness 500±10μm) was cut into ~15×15 mm^2 squares with a diamond pen. The polished side was used for device fabrication, which required no scratches and no pollution. Placed the p-doped silicon in the acetone solution with the smooth-bright side up and ultrasonically cleaned for about 1 hour. Then ultrasonicated the p-Si substrate in ethyl alcohol and deionized water for about 40 minutes respectively. Finally, the p-Si surface was blow-dried and stored in selfadsorption rubber box before used.

For PEO/ITO structure, the substrate ITO (with sheet resistivity 4 ~ 7 Ω, light transmittance 78% and thickness ~1.1mm) was cleaned similar to Si substrate. First, the ITO surface was wiped with alcohol. Then ultrasonicated in acetone, ethyl alcohol and deionized water for about 30 minutes respectively. Before fabricating the devices, the ITO was exposed under UV in an ozone environment for 15 min.

2.3.2 Solution preparation

Complexed the lithium salt (LiTFSI, powder) and poly oxyethylene (PEO, powder, contains 200-500 ppm BHT as inhibitor) with a certain molar ratio of EO and Li^+ (EO:Li). Dissolved the LiTFSI and PEO in appropriate amount of acetonitrile (ACN) to gain Li-PEO solution. If to get Li-PEO-SiO_2 solution, added SiO_2 nanoparticles into the solution with certain weight percentage. The solution was stirred with a magnetic stirring apparatus for 24 hours at ambient temperature to get the homogenous solution. Ultrasonic dispersion can be used as an auxiliary method to get homo-dispersed solution.

2.3.3 Electrolyte membrane preparation

The substrate is vacuum fixed on the spin coater and several drops of the prepared solution (~100 μL) was dropped on the substrate by a plastic dropper. Then a nanoscale thickness-film was spun on the p-Si substrate surface by spin-coating method mentioned in section 2.2.1 with proper rotating speed. Cured the membrane at set temperature on simple hot plate for over 2 hours to completely volatilize the solvent.

2.3.4 Deposition of top electrode

After curing, the top electrodes were deposited on the electrolyte film by thermal evaporation (High vacuum resistance evaporation coating equipment) through a shadow mask. For thermal evaporation, the target materials are placed in inert metal boat at the bottom of the evaporation cavity. By applying power to the boat connected to the power source, it can generate enough heat to melt and evaporate the solid material in board and then deposit on the substrate at a set rate. The deposition rate is related to the film-forming ability and the interfacial diffusion of the material. The shape of the deposited ones is consistent with the stainless steel mask. High vacuum can prevent the material from being oxidized during evaporation. Here, silver particles or gold wire were used as the target material to form films with certain thickness and circular pattern.

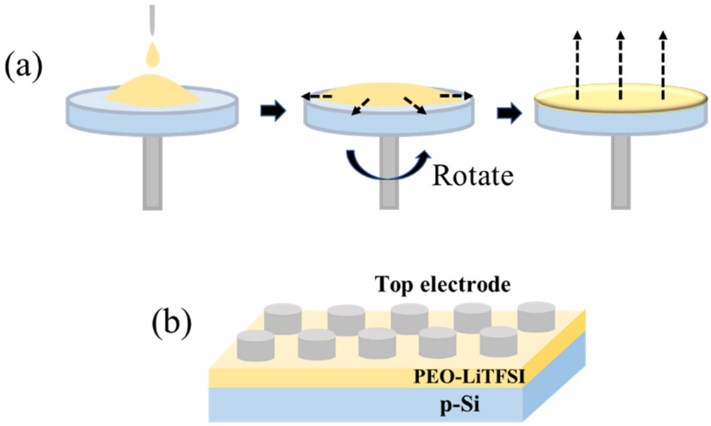

Fig. 2.1 (a) Schematic of the spin-coating process. (b) Schematic of the fabricated memristor devices

The schematic of the fabricated memristor is shown in Fig. 2.1(b). The process of solution preparing, spin-coating and curing process were all conducted in glove box with filled with Ar gas (water content < 0.01 ppm and oxygen content < 0.01 ppm). The top electrode deposition process was conducted in vacuum.

2.3 Structural and morphological Characterization method

2.3.1 Surface profilometer

Surface profilometer, or step-meter, is a contact-type surface topography measuring instrument. According to the different sensors used, the surface profilometer can be divided into three types: inductive, piezoelectric and photoelectric. When the stylus slides along the measured surface gently, due to the tiny peaks and valleys or pits on the surface, the stylus moves up and down along the surface of the sample while sliding, thus the motion of the stylus can reflect the surface contour.

The surface profilometer has the advantages of high measuring accuracy, large measuring range, stable and reliable measuring results and good repeatability. By processing the signal, it can also reduce the noise of the information, amplify signal and so on.

In the experiment, surface profilometer (Alpha-step D-600) was used to measure the thickness of the Li-PEO electrolyte membrane spun-coated on the p-Si substrate. The stylus force equals to 0.03mg.

2.3.2 Atomic force microscope (AFM)

Atomic force microscopy (AFM) can characterize the surface morphology of the film and the average roughness of the selected area can be read from the value of RMS.

The AFM uses a very sharp tip (microcantilever) to measure and magnify the force between the tip probe and the atoms under test, so to probe and map the topography of the samples. It has atomic resolution and suitable to detect various kinds of materials. There are three different AFM modes employed: contact mode, noncontact mode, and tapping mode. For the contact mode, the tip of the microcantilever scans the surface in close contact with the sample, causing high wear rate and failure during the scanning process. Contact mode AFM is the most commonly used surface force measurement method[62]. For the noncontact mode, the tip of the microcantilever usually lingers 5~15 nm above the sample surface, being not accurate enough for surface roughness characterization. As for tapping mode AFM, the tip "knocks" on the sample with only instant contact, solving the influence of friction, adhesive force, electrostatic forces and other disadvantages caused by the tip being dragged over the sample. Meanwhile, the AFM need no special treatment of the sample, avoiding irreversible damage to the sample. AFM can also provide three-dimensional surface mapping compared with SEM.

In the experiment, we used AFM (MFP-3D, Oxford Instruments) to characterize the roughness of the Li-PEO membrane spun-coated on the p-Si substrate.

2.3.3 Scanning Electron Microscope (SEM)

Scanning electron microscopy (SEM) uses focused high-energy electron beams to generate various signals on the surface of a solid sample. The accelerated electron beams in SEM carry a large amount of kinetic energy. When the incident electrons decelerate in the sample, these energies are dissipated as various signals generated due to the interaction between electrons and sample. These signals indicate the information about the sample, including secondary electrons (reveal the morphology or topography and produce SEM image), backscattered electrons (BSE, illustrate contrasts in composition of multiphase samples), diffracted backscattered electrons (EBSD, determine the crystal structures and orientations), photons, light and heat.

In most applications, data is collected on selected areas and a two-dimensional image is generated, showing spatial variations. For some sample with low conductivity, conductive coating is needed before electronic scanning to improve electrical conductivity, so as to get a better SEM image.

In our experiment, we used SEM (Mira3, with accelerating voltage 5.0 kV) to characterize the micro-morphology of the membranes spun-coated on the substrates. An ultrathin platinum was deposited on the surface before testing to improve the conductivity of the samples.

2.3.4 Energy Dispersive Spectrometer (EDS)

In SEM and transmission electron microscopy (TEM), energy dispersive spectrometer (EDS) is an important attachment, which is suitable to analyze the chemical elements in a microscopic volume in the specimen since the electron probe can be focused on a very small area[62]. With EDS in EM, elemental analysis can be obtained while examining the microstructure.

Each element has its own characteristic X-ray wavelength, which depends on the characteristic energy released during energy level transition. And EDS is used to separate the characteristic X-rays of different elements into energy spectrum. EDS can be used for qualitative and quantitative analysis. In quantitative analysis, the concentration of the various elements is obtained by X-ray intensity and the intensity ratio is usually converted into the concentration ratio by quantitative correction according to the actual situation.

Here, we used EDS (Mira3, with accelerating voltage 20.0 kV) to analyze the type and content of component elements in the Li-PEO(-SiO_2) membrane.

2.3.5 X-ray Diffraction (XRD)

XRD, which has been widely used in physics, chemistry, earth science, material science and many other fields, can be used for phase analysis, crystallinity determination, precise lattice parameters determination and so on. It is non-destructive to the sample and suitable for various materials. XRD works by illuminating the sample with incident X-rays and then measuring the scattering angle and intensity of the outgoing X-rays irradiated. When a beam of monochromatic X-ray crystal is incident, the distance between the atoms in the regular arrangement is of the same order with the magnitude of the incident X-ray's wavelength, and they interfere with each other, resulting in strong X-ray diffraction in some special directions. The orientation and intensity of the diffraction line in space distribution thus can reflect the crystal structure.

In 1913, British physicists W.H. and W.L.Bragg proposed the Bragg's Law on the basis of Laue's discovery:

$$2d \sin\theta = n\lambda \qquad (2-1)$$

where d is the interplanar spacing, θ is the incidence angle of X-ray, n is the diffraction order and λ is the wavelength of the characteristic X-ray. Bragg's Law is the basis of crystal diffraction and XRD.

To calculate the relative crystallinity χ, the equation below is used[63]:

$$\chi = \frac{I_{crtstal}}{I_{total}} \times 100\% \qquad (2-2)$$

where $I_{crtstal}$ is the crystal diffraction intensity (sum of the diffraction intensity of each peak) and I_{total} is the total diffraction intensity. So, integrated the area of crystalline peaks and total area with Origin software and calculated the relative crystallinity.

Here, we used XRD to mainly characterize the relative crystallinity of the films. The target material is Cu. The 2θ changed from 10° to 90°, with scanning rate of 5°/min.

2.4 Electrical Characterization and analysis method

2.4.1 Electrochemical Impedance Spectroscopy (EIS) and ionic conductivity

Electrochemical impedance spectroscopy (EIS) can be used to analyze kinetics of electrode process, double electric layer, diffusion process and so on by recording the change of impedance with the sine wave frequency, and then it can be used to study the mechanism of electrode materials, solid electrolyte, conductive polymer and corrosion protection.

Take the electrochemical system as an equivalent circuit, apply a small amplitude alternating potential wave with changing frequencies, and measure the ratio of the alternating potential to the current signal (Ω, which is the system's impedance) with the change of sine wave frequency (ω), or with the change of the phase angle of the impedance (Φ). One feature of EIS over other transient techniques is that only an infinitely small sine wave perturbation is required to be applied to the steady-state system, which do not result in large changes in the membrane structure[64].

The ionic conductivity can be evaluated by EIS results. By analyzing the equivalent circuit, the bulk resistance, interface resistance and other resistances of the solid polymer electrolyte can be measured, which can further analyze the ionic conductivity.

Before EIS test, assembled CR3032 button cell in the glove box, with O_2 content < 0.01 ppm and H_2O content < 0.01 ppm. For the cell, the thin membrane to be test was sandwiched between tow stainless steels as stainless steel is blocking electrode for Li ions. And the subsequent analysis of the EIS spectra of stainless steel-symmetrical button cell would be simpler and more intuitive. Ionic conductivity σ can be calculated by the following equation[65]:

$$\sigma = \frac{d}{SR} \qquad (2-3)$$

where d is the thickness of electrolyte film, S is the contact area between electrolyte and blocking electrode, and R is the body resistance of the electrolyte film. To measure the thickness d, first measure the thickness of two stainless steel sheets before assembling them into cell. After the test is completed, disassemble the cell and measure the stainless steel sheets with polymer film between them. Take the difference between the two measured values and denoted it as d.

In the experiment, the Li-20PEO membrane and Li-20PEO-SiO_2 membrane were assembled into stainless steel symmetric button cell and gained the EIS spectra as well as the fitting equivalent circuit, finally calculated the ionic conductivity of the membranes.

2.4.2 DC current-voltage (I-V) sweeping and resistance switching

DC current-voltage (I-V) sweeping, or cyclic voltammetry scanning, is one basic and important method to characterize the electrical properties, like the resistance switching phenomena of memristors. Generally, the DC I-V sweeping is conducted with semiconductor analyzer equipped with probe station. Two probes were used for the I-V sweeping, one attached to the top electrode and the other attached to the bottom electrode. According to the experimental requirements, apply positive or negative bias on top electrode and repeat the sweeping process for several times or hundreds of times. To test the stability of the resistance switching, at least 50 cycles of I-V sweeping should be conducted. By analyzing the I-V sweeping results, we could know more about the RS and resistance changing behaviors of the devices.

The DC I-V sweeping is conducted with Keithley Semiconductor Parameter Analyzer (4200A-SCS and 2400 SMU) equipped with Semiconductor Variable Temperature Probe System and microscope with CCD. By selecting different modules of the analyzer, such as resistor module, capacitor module and three-terminal transistor module, various electrical properties of the device can be tested. For memristors, the resistor module can be used to represent the basic current versus voltage or time diagram. There are also some programmable modules, which can set the waveform, amplitude, width and period of the input electrical signal to meet the requirement of different testing.

Here, all devices underwent I-V sweeping to analyze their RS properties and further to analyze the RS mechanism.

Chapter 3 Preparation and Properties of Nanoparticles-Doped Li-Ion Memristors

3.1 Introduction

SPE with Li salt has many advantages like light weight, good processability and interfacial wettability, gaining more and more interest. Using Li salt to prepare the electrolyte membrane can achieve many advantages like multiple resistance levels[49], large programmable range with continuous resistance states, symmetrically reading and strong data retention[48]. The commonly used Li salt includes $LiClO_4$, $LiNbO_3$ and so on, but seldom LiTFSI.

To further improve the ionic conductivity of SPE with Li at ambient temperature (10^{-6}~10^{-9} $S{\cdot}cm^{-1}$), some nano-filler can be doped to enlarge the amorphous region of Li-PEO electrolyte, then to influence the ionic conductivity. The electrolyte doped with nano fillers thus can perform differently in memristive behaviors.

Here, to increase the ionic conductivity and decrease the working power consumption, nano SiO_2 (average diameter ~10 nm) was added into the Li-PEO electrolyte. Two Li-ion based memristor devices with inert gold electrode were fabricated, marked as Au/Li-20PEO/Si and Au/Li-20PEO-SiO_2/Si. The membrane preparation methods include spin-coating and solution-casting. After drying, characterized the Li-20PEO and Li-20PEO-SiO_2 membranes by different methods and tested the current-voltage (I-V) properties of the devices to study the resistance switching behaviors and mechanism. As the I-V property under unipolar bias has certain similarities with synapse, here we also test the output current with unipolar electrical bias. Finally, the power consumption was calculated and the resistance switching mechanism is put forward.

3.2 Experiments

3.2.1 Fabrication of the Li-ion based memristor

Prepared the solution. A certain amount of LiTFSI powder was mixed with PEO powder, with a certain ratio of EO:Li. To prepare the nano-SiO_2 doped film, SiO_2 with certain weight percentage was added as well. Then dissolved the mixture in acetonitrile in the glove box filled with Ar gas (water content < 0.01 ppm and O_2 content < 0.01 ppm). Then stirred the solution with magnetic stirring apparatus for 24h.

Spin-coating method to fabricate electrolyte membrane. First to clean the substrate. The p-doped Si substrate was ultrasonically cleaned in acetone for 40 min, ethanol for 30 min and deionized water for 20 min in sequence. The solution was then spin-coated on the substrate p-Si in the glove box, and cured at 40°C to 60°C for 2 hours. The membrane is transparent or semi-transparent.

Fabricated the device. After curing, gold with thickness of ~68 nm was deposited on the Li-PEO or Li-PEO-SiO_2 film by thermal evaporation through a shadow mask as the top electrode. There are three sizes of the pattern on the mask, so electrodes have the diameter of ~70μm, ~100μm and ~200μm. Finally, the effective area of the memristor devices, which equals to the area of the electrode deposited, was about $70\times70\ \mu m^2$, $100\times100\ \mu m^2$ and $200\times200\ \mu m^2$.

3.2.2 Single-step and multi-step spin-coating method

First adopted the single-step spin-coating method with high rotate speed directly (2500 rpm or 5000rpm for 60 s) to prepare the membrane on the substrate. But the membrane fabricated with this method has large thickness, which is undesired due to the long distance ions should travel across. So then changed it to the multi-step spin-coating method, in which applied lower rotate speed (500 rpm) at first then followed by a higher speed (2500 rpm or 5000rpm). With multi-step spin-coating method, the thickness of the membrane greatly decreases form ~1.5 μm to ~300 nm (up to 80%), as shown in Table 3.1.

Table 3.1 Thickness with different spin-coating method

	Coating parameter	Thickness
Single-step spin-coating	2500 rpm, 60 s	1.5 um
	5000 rpm, 60 s	1.1 um
Multi-step spin-coating	500 rpm, 20s + 2500 rpm, 60 s	352 nm
	500 rpm, 20s + 5000 rpm, 60 s	173 nm

3.2.3 Preparation of the thicker Li-ion electrolyte membrane

For some characterization like XRD and EIS, a thicker film was needed. Here, solution casting method was used to prepare the film. The preparation of the solution was the same as section 3.2.1. The as-prepared solution was poured into polytetrafluoroethylene mode and curing at ambient temperature for more than 48 hours in glove box to evaporate the solvent thoroughly. After fully drying, the film was then peeled off from the mold and did the subsequent measurements. Fig. 3.1 is the photos of pure PEO, Li-20PEO and Li-20PEO-SiO_2 membrane. Since the membrane prepared by this method has larger thickness, it shows nearly no transparency.

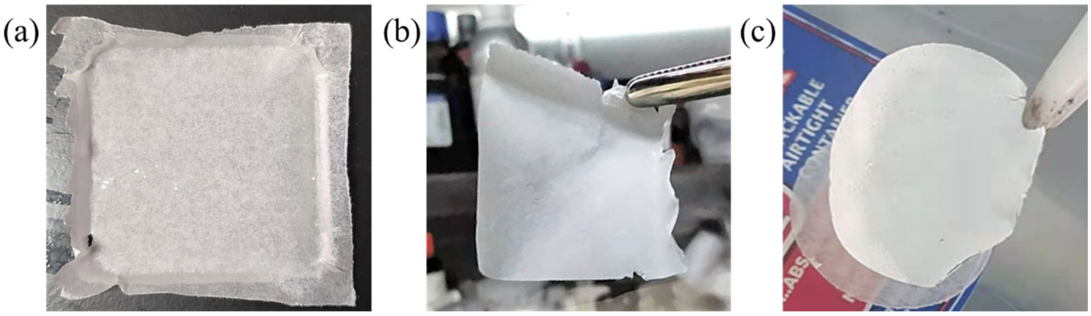

Fig. 3.1 Photos of (a) pure PEO membrane before peeling off the mold, (b) Li-20PEO membrane and (c) Li-20PEO-SiO_2 membrane after peeling

3.2.4 Testing and characterization

SEM was tested to measure the micro morphology of the electrolyte membrane. Also, the elemental composition on the surface of the electrolyte films can be confirmed by EDS.

XRD test was conducted to characterize crystallinity of the electrolyte membrane. The target material is Cu. The scanning range was from 10° to 90°, with a scan rate of 5°/min. The silt widths were both 1/2.

EIS test with electrochemical workstation was used to measure the ionic conductivity of the electrolyte membrane. To measure the ionic conductivity of Li-20PEO and Li-20PEO-SiO_2 membrane, the fully dried Li-20PEO and Li-20PEO-SiO_2 films fabricated by solution casting method were cut into circular pieces with diameter about 20 mm and sandwiched between two stainless steel disks (with diameter of 15.8 mm) as blocking electrodes in the glove box, assembling into a button symmetric cell, recorded as Fe|Li-20PEO|Fe and Fe|Li-20PEO-SiO_2|Fe. Before conduct the EIS measurement, the Fe|Li-20PEO|Fe cell was heated to 60 degree for several minutes and cooled to ambient temperature, to improve the interfacial contact and obtain a more precise result. The Fe|Li-20PEO-SiO_2|Fe cell was also subjected to EIS test at different temperature (room temperature and 60 degree) to improve the interfacial contact. The thickness of the electrolyte membrane was measured with micrometer calipers.

DC I-V sweeping was used to characterize the electrical properties of the memristor devices with electrochemical workstation (4200A-SCS parameter analyzer) equipped with Probe Station. The DC I-V sweeping was conducted with different electrode size at ambient temperature and in the atmosphere. When analyzing the I-V property, the data is shown in single-logarithmic coordinate or linear coordinate as needed. The absolute values are usually adopted to plot in the logarithmic coordinate. In this chapter, unless otherwise noted, the figures are drawn in linear coordinates. At each I-V cycles, the maximum current usually appears at largest voltage, to compare the conductance level, the maximum values (with same cut-off voltage) were recorded.

The working power consumption of memristor was calculated from the I-V curve, according to the equation below:

$$P = \int VdI \tag{3-1}$$

where P is the power, V is the voltage and I is the current. To compare the power consumption, take the integral of I-V curve at positive bias. The calculation process was taken with the integral function Origin software.

3.3 Structure and morphology analysis

3.3.1 Crystallinity and structure analysis: XRD

Fig. 3.2 is the XRD spectra of films with different EO:Li ratio. As illustrated in Fig. 3.2, more addition of Li salt in PEO (lower EO:Li ratio) will cause lower crystallinity except EO:Li = 20. For EO:Li=25, 15, 10, 8, the intensity of characteristic peaks of PEO (2θ ~ 19° and 23°) decreases and the broad XRD background region enlarge gradually. However, the film with EO:Li=20 has lowest intensity of characteristic peaks and widest broad XRD background region, which related to the lowest crystallinity. Since Li ions moves by complexing with EO groups, the ratio of

EO:Li directly affects the binding and velocity and crystallinity[66]. In other word, the amount of Li should be not too much or too less due to the certain coordination number of EO-Li. Thus, proper Li salt concentration (EO:Li=20 in our case) can lead to optimum crystallinity.

Meanwhile, with different ratio of EO:Li, the film-forming ability of the solutions are different. Among the ratio mentioned above, the film-forming ability with EO:Li=20 is best, solidifying into a free-standing film. The solutions with other ratios were unable to form peelable film, showing that too high or too low ratio of EO:Li is unfavorable to form free-standing film[67]. So, in the subsequent tests of the memristor device, the ratio of EO:Li remained at 20.

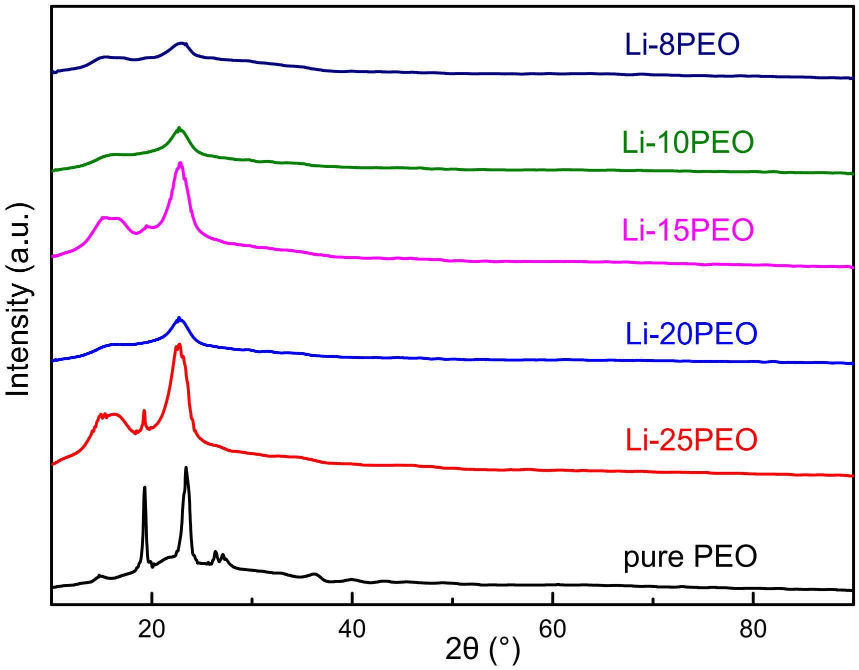

Fig. 3.2 XRD patterns of the films with different EO:Li ratio: pure PEO (black line), Li-25PEO (red line), Li-20PEO (blue line), Li-15PEO (purple line), Li-10PEO (green line) and Li-8PEO (dark blue line). Scanning range of 2θ: 10° to 90°, with scan rate of 5°/min

Fig. 3.3 shows the XRD patterns of the pure PEO, Li-20PEO and Li-20PEO-SiO_2 membrane simultaneously. For pure PEO, two characteristic peaks are observed at 2θ

~ 19° and 23°, consistent with the literature[68, 69]. The broad XRD background indicates the amorphous or semi-crystalline structure of the PEO film. For Li-20PEO and Li-20PEO-SiO_2, the decreased peaks at 2θ ~ 19° and 23° demonstrate the lower crystallinity of the film. Meanwhile, the larger broad XRD background region represents the reinforced amorphous phase region of PEO. Li-20PEO-SiO_2 film has lower signal intensity than that of Li-20PEO, and the relative crystallinity can be calculated form equation (2-2), which is 8.95% for pure PEO, 4.32% for Li-20PEO and 1.92% for Li-20PEO-SiO_2. It demonstrates that the addition of nano SiO_2 particles (average diameter = 10 nm) further reduces the crystallinity.

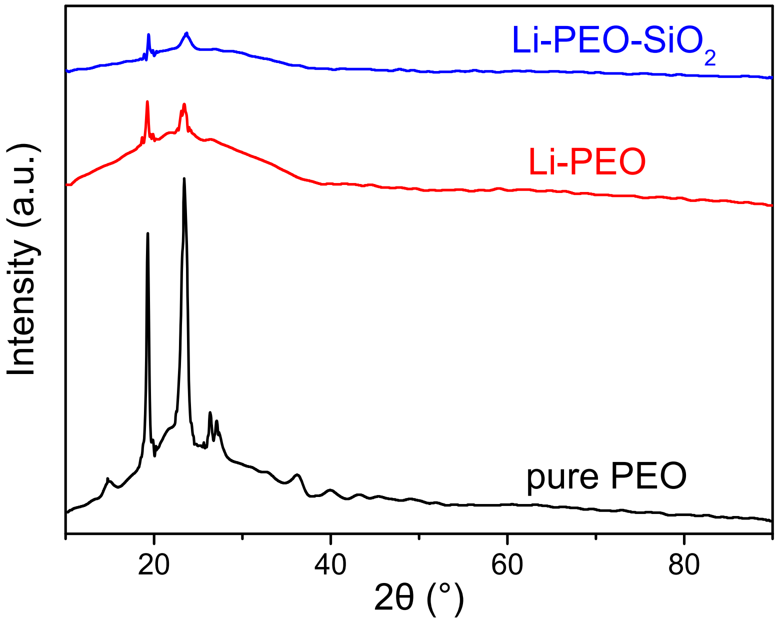

Fig. 3.3 XRD patterns of pure PEO, Li-20PEO and Li-20PEO-SiO_2 in the range of 2θ from 10° to 90°, with scan rate of 5°/min

3.3.2 Surface morphology: SEM

Fig. 3.4 is the scanning electron microscope (SEM) image of the fabricated PEO electrolyte film with magnification of 2,000× (Fig. 3.4a) and 4,000× (Fig. 3.4b). The surface of the PEO film is flat with no significant defect. Some grain boundary can be seen from SEM images. From the SEM image, we may consider it locally homogeneous and dense.

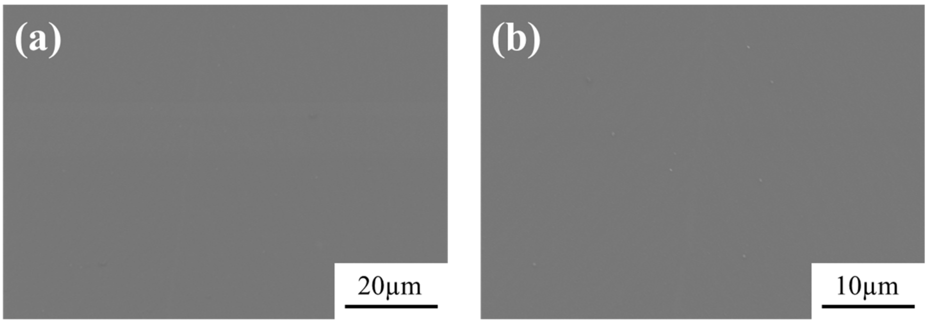

Fig. 3.4 SEM image of pure PEO film spin-coated on the p-Si substrate. The magnification of (a) is 2,000× and that of (b) is 4,000×

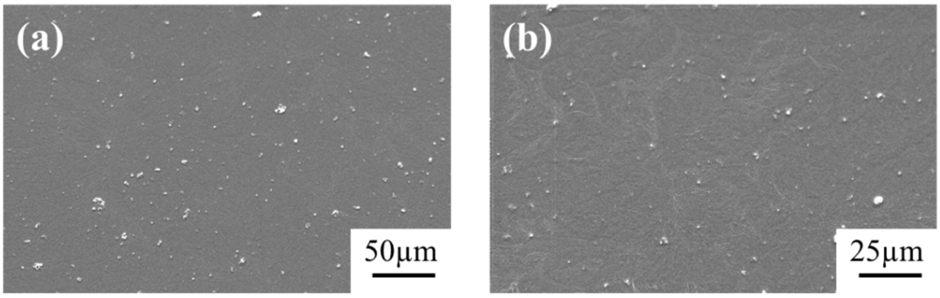

Fig. 3.5 SEM image of Li-20PEO film spin-coated on the p-Si substrate. The magnification of (a) is 500× and that of (b) is 1,000×. (a) and (b) correspond to the same area of the sample

Fig. 3.5 is the SEM image of the Li-20PEO film spin-coated on the p-Si substrate with magnification of 500× (Fig. 3.5a) and 1,000× (Fig. 3.5b), and these two images correspond to the same area of the sample. At relative low magnification (Fig. 3.5a), the film is flat on the whole with some participated LiTFSI particles due to the high hygroscopicity and agglomerative property of LiTFSI[61]. While at relative high magnification (Fig. 3.5b), a wrinkle caused by the electron beam can be seen, which may be cause by electron beam disruption. Since the high energy electron beam will damage the polymer film, this Li-20PEO film cannot take SEM image with too high magnification.

3.3.3 Element distribution: EDS

Fig. 3.6 and Fig. 3.7 are the EDS mappings of Li-20PEO and nanoparticle-doped Li-20PEO-SiO_2 with elements F, S, Si, O, and C. There is no Li mapping because that the element Li is too light to be detected through EDS. As depicted in Fig. 3.6, F and S elements, from Li salt (LiTFSI), are evenly distributed on the surface of the film, suggesting the uniform distribution of LiTFSI in the Li-20PEO film.

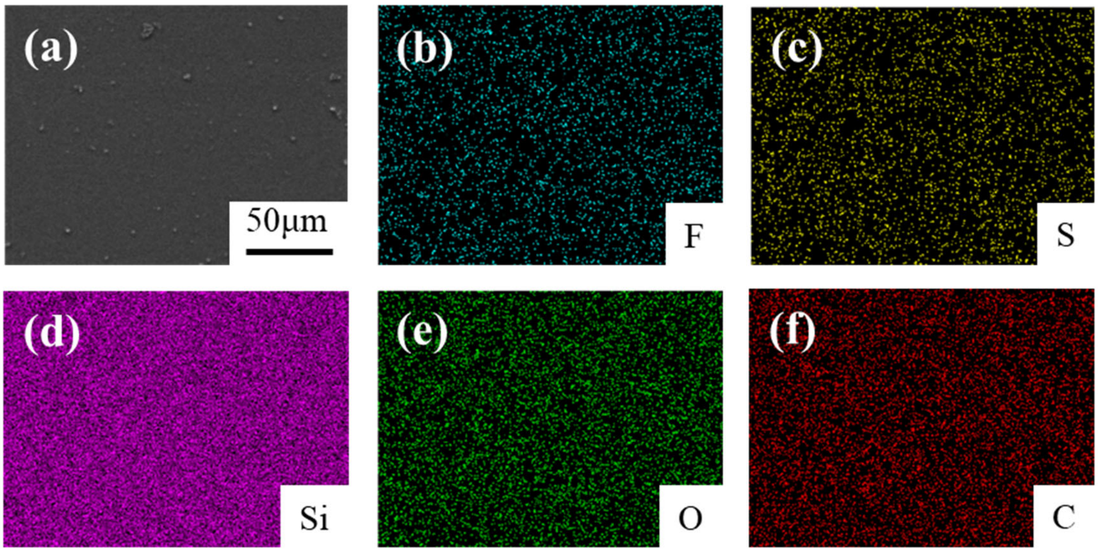

Fig. 3.6 EDS mapping of Li-20PEO spin-coated on p-Si. (a) SEM image of information collection area. (b) ~ (f) are F, S, Si, O and C elements respectively

For Li-20PEO-SiO_2 film, some distinct particle aggregation was observed as shown in Fig. 3.7(a). To further distinguish the chemical component of the particle, EDS mapping was made. As shown in Fig. 3.7, the O content is much higher on the particle surface. The Si content is lower because compared with the Si substrate, SiO_2 aggregation has relatively low Si content. At the same time, element S, F and C distribute slightly intensively, meaning the affinity of Li-PEO composite to SiO_2. The aggregation may adverse to the performance of the devices.

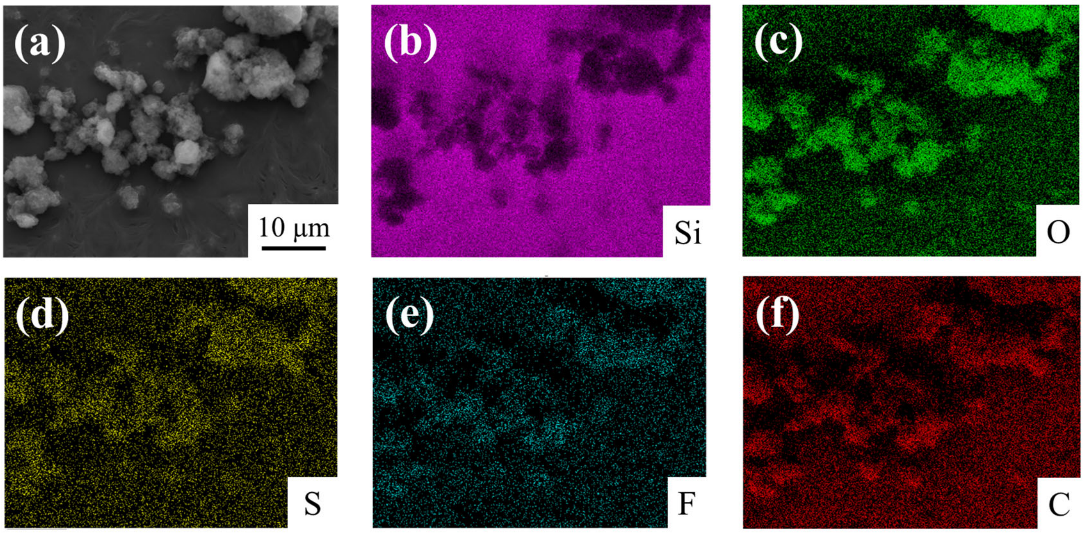

Fig. 3.7 EDS mapping of Li-20PEO-SiO_2 spin-coated on p-Si. (a) SEM image of information collection area. (b) ~ (f) are Si, O, S, F, and C elements respectively

3.3.4 Thickness and roughness

The thickness measured by surface profilometer and roughness measured by atomic force microscope (AFM) were summarized in Table 3.2. All of the films were fabricated with multi-step spin-coating. Fig. 3.8 is the AFM results of (a) pure PEO, (b) Li-20PEO and (c) Li-20PEO-SiO_2 film spin-coated on p-Si substrate. The average roughness can be read from the AFM results, which are ~14.385nm for pure PEO, ~0.776133nm for Li-20PEO and ~ 1.37273nm for Li-20PEO-SiO_2. For pure PEO, it has high viscosity. Addition of Li salt can decrease the viscosity and makes the solution form a more uniform film during the curing process, resulting in lower roughness. The roughness of these three sorts of films is small enough for the device which requires high uniformity, indicating that the films prepared by previous method can be initially applied to the memristor device.

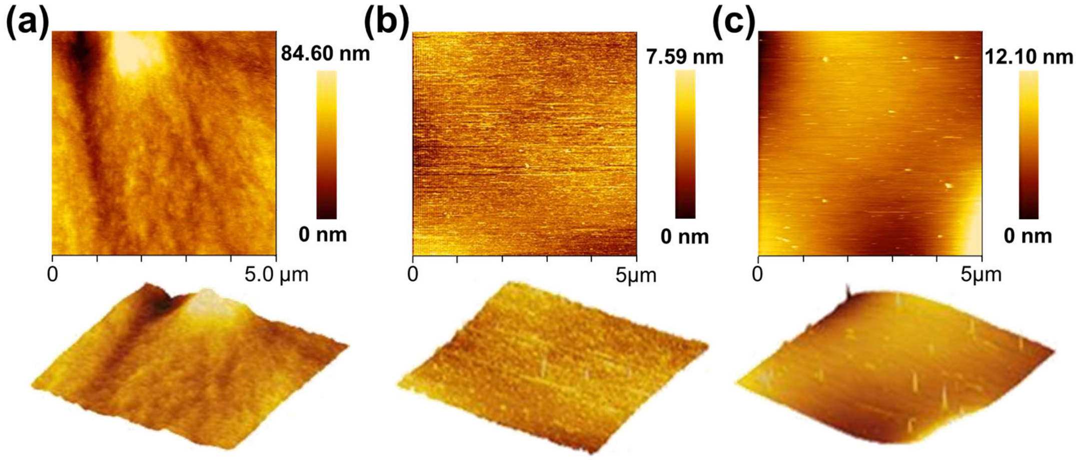

Fig. 3.8 AFM results of (a) pure PEO, (b) Li-20PEO and (c) Li-20PEO-SiO_2 film spin-coated on p-Si. The average roughness of (a) is ~ 14.385nm, (b) is ~ 0.776nm and (c) is ~ 1.373nm

Table 3.2 The thickness and roughness of the pure PEO, Li-20PEO and Li-20PEO-SiO_2 film

Composition of film	Thickness	Roughness
Pure PEO	~ 180 nm	~ 14.385nm
Li-20PEO	~ 60.0 nm	~ 0.776nm
Li-20PEO-SiO_2	~ 23.0 nm	~ 1.373nm

3.3.5 Analysis of ionic conductivity: EIS

The EIS spectra of Fe|Li-20PEO|Fe symmetric cell are plotted in Fig. 3.9, the insert was the fitting equivalent circuit. The Nyquist plot, as depicted in Fig. 3.9, consists of a semi-circular arc in high frequency region and a diagonal line in low frequency region. The former one is related to the electrolyte body resistance Rb and the geometric capacitance C1, while the diagonal line is related to the electrolyte/electrode interface capacitance CPE1 (constant phase angle element).[70] The ionic conductivity calculated by equation mentioned in chapter 2 is 1.78×10^{-5} S/cm, comparative with the ionic conductivity of common polymer[70].

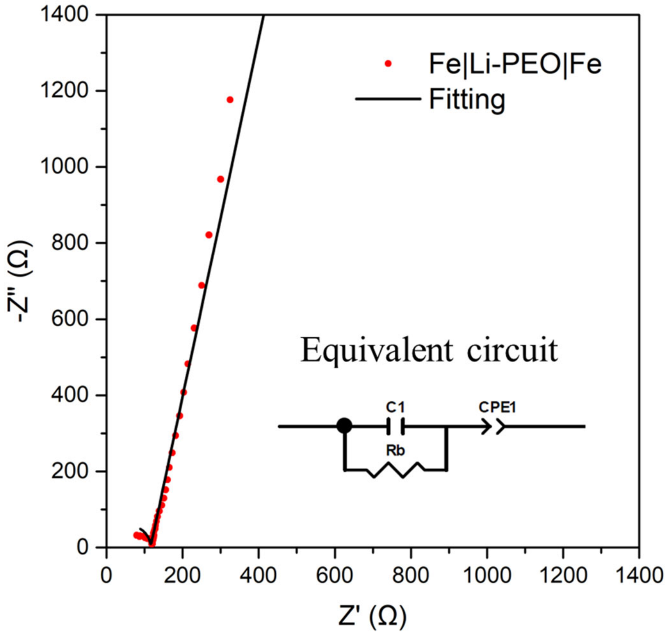

Fig. 3.9 EIS spectra and equivalent circuit of Fe|Li-20PEO|Fe symmetric cell

Fig. 3.10 is the Nyquis plot and the corresponding equivalent circuit of Fe|Li-20PEO-SiO_2|Fe symmetric cell at room temperature and 60°C. As discussed for Fe|Li-20PEO|Fe, the Nyquist plot in Fig. 3.10 also consists of a semi-circular arc and a diagonal line. The ionic conductivity calculated is 5.56×10^{-6} S/cm at room temperature and 6.38×10^{-6} S/cm at 60°C. Compared with Li-20PEO membrane, the slight decreased ionic conductivity Li-20PEO-SiO_2 may be caused by the interactions between surface hydroxyl groups of SiO_2 nanoparticle and anions of lithium salt[71]. In this case, $TFSI^-$ may form F~H-O type hydrogen bounds. The enlarger free space near SiO_2 surface also acts as adsorption center, further hindering the movement of anions, therefore showing an overall lower ionic conductivity of Li-20PEO-SiO_2 membrane.

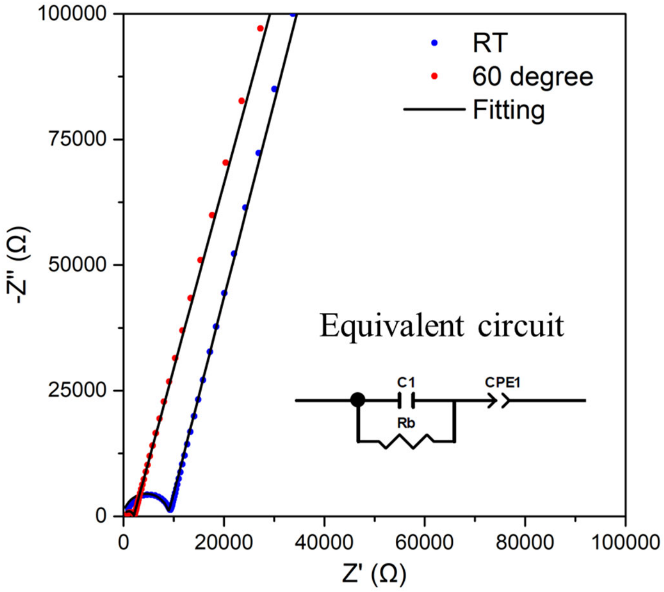

Fig. 3.10 EIS spectra and equivalent circuit at room temperature (RT) and 60°C of Fe|Li-20PEO-SiO_2|Fe symmetric cell

3.4 Current-voltage characteristics analysis

3.4.1 Electrical response with different sizes of the electrode

The device may response differently with different electrode size. After deposition of the top electrode, the electrode size was measured with optical microscope, which are 201.07μm (~200 μ m), 105.38μm (~100μm) and 77.42μm (~70μm) respectively. Then the devices were subjected to I-V scans.

With same cut-off voltage, the maximum current value of Au/Li-20PEO/Si and Au/Li-20PEO-SiO_2/Si under negative and positive bias was counted and the average value was summarized in Table 3.3. Whether or not adding the nano SiO_2, the maximum current at both negative and positive increases with larger electrode size, as shown in the table. The size of the electrode is almost equal to the effective area of the device, so larger electrode size means larger effective area and more available conductive ions in the electrolyte, thus showing larger current during cycling.

In reality, high density information storage requires small device size and small working current as well. But the difference between electrodes is tolerable in experiment, so the largest electrode was selected as the major testing ones to get larger and more accurate response current.

Besides, with same cut-off voltage of ±2V, the maximum current of Au/Li-20PEO-SiO_2/Si is smaller than that of Au/Li-20PEO/Si. The result is consistent with the lower ionic conductivity discussed in section 3.3.

Table 3.3 Maximum current under negative and positive bias for Au/Li-20PEO/Si and Au/Li-20PEO-SiO_2/Si. (Cut-off voltage: ±2V. Unit: mV.)

	Au/Li-20PEO/Si		Au/Li-20PEO-SiO_2/Si	
Size of electrode	Maximum current at negative bias (mV)	Maximum current at positive bias (mV)	Maximum current at negative bias (mV)	Maximum current at positive bias (mV)
~70μm	-7.0×10^{-5}	4.5×10^{-5}	-1.00×10^{-5}	1.00×10^{-5}
~100μm	-8.0×10^{-5}	6.0×10^{-5}	-1.30×10^{-4}	1.30×10^{-4}
~200μm	-1.8×10^{-4}	2.2×10^{-4}	-1.40×10^{-5}	1.35×10^{-4}

3.4.2 Current-voltage characteristics of Au/Li-20PEO/Si

Fig. 3.11 is the DC current-voltage properties of Au/Li-20PEO/Si. With small cut-off voltage (±1.0V), the trend is erratic and the resistance become higher under both positive and negative bias, as illustrated in Fig. 3.11(a). With larger cut-off voltage (±2.0V) in Fig. 3.11(b), SET behavior appears under positive bias (SET voltage ~2V) and RESET behavior under negative bias (RESET voltage ~-0.5V), but with noise of data. The current will return to zero at non-zero voltage, which is threshold switching (TS) related to the unstable and vulnerable RS behavior. Under small cut-off voltage, the resistance changes within a small range. Then the cut-off voltage was enlarged to ±5.0V, the SET and RESET behaviors become steadier, with SET voltage ~2V. And the ON/OFF ratio can reach about 10^5 at positive bias. The result indicates that for Au/Li-20PEO/Si, larger cut-off voltage is needed to pursue legible RS behaviors with large ON/OFF ratio.

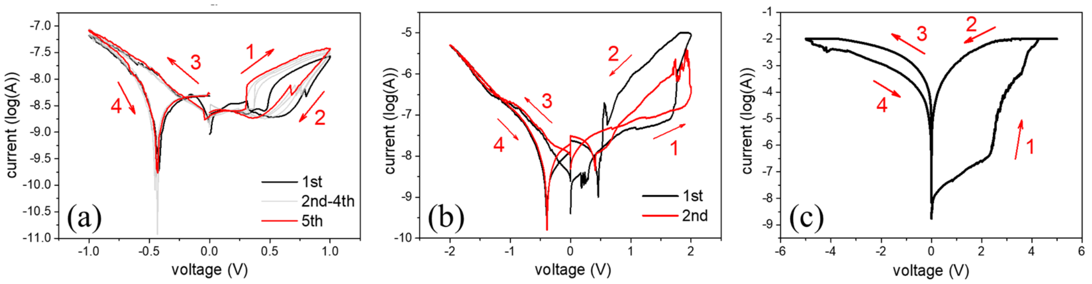

Fig. 3.11 DC current-voltage sweeping of Au/Li-20PEO/Si in logarithmic coordinates. The sweeping range is (a) 0 → 1.0V → -1.0V→ 0V, (b) 0 → 2.0V → -2.0V→ 0V, (c) 0 → 5.0V → -5.0V→ 0V

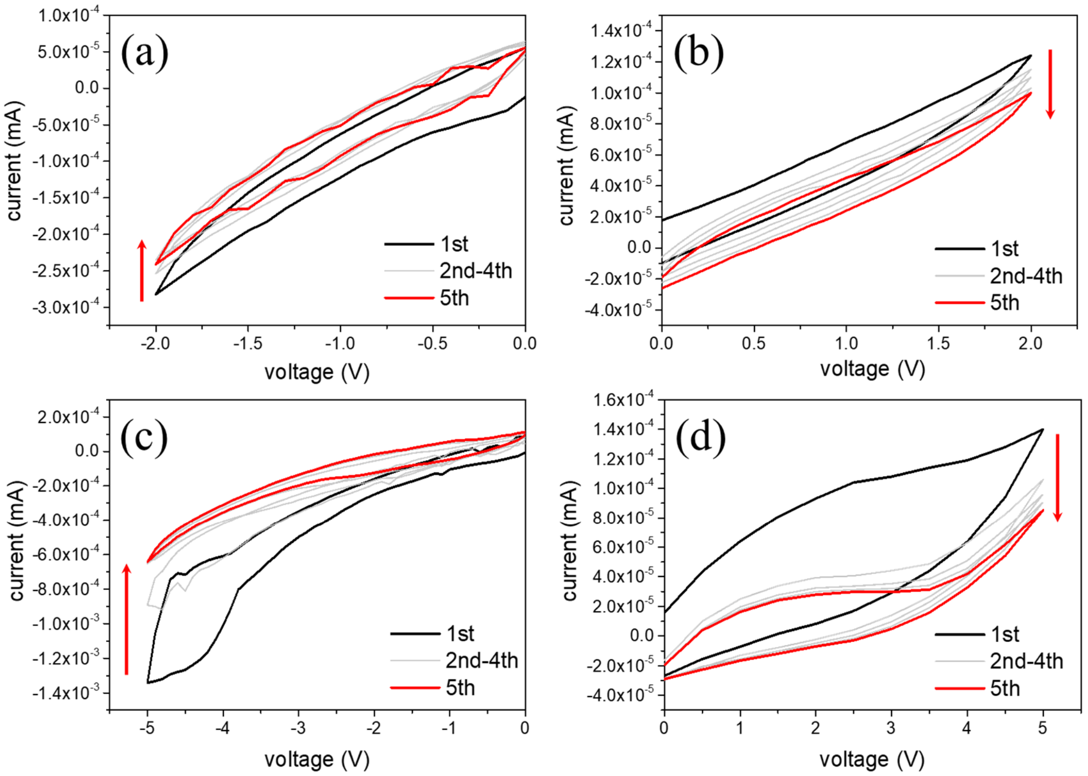

Fig. 3.12 Unipolar DC I-V sweeping of Au/Li-20PEO/Si. Negative bias from (a) 0 → -2.0V→ 0V and (c) 0 → -5.0V→ 0V. Positive bias from (b) 0 → 2.0V→ 0V and (d) 0 → 5.0V→ 0V

To study the electric response under unipolar bias, applied consecutive unipolar bias (±2.0V and ±5.0V) on Au electrode, and the results are shown in Fig. 3.12. No matter the polarity or the amplitude of the external bias, the current decreases with each cycle, as the arrow shows. It means the 1st cycle activates the devices but the subsequent ones cannot induce more ions to migrate. And the conductive and movable ions are consumed, resulting in gradually minishing current from 1st cycle to 5th cycle. There is no significant switching (SET or RESET) behavior but shows changing resistance states while cycling, which is called memristive type as mentioned in chapter 1. The devices with switching behavior can be used in digital data storage while the memristive ones can be used in analog data storage due to its multiple levels of resistance state[11]. Fig. 3.11 and Fig. 3.12 also demonstrate the switching and memristive can convert into each other under appropriate conditions.

Under different voltage, the difference of the HRS and LRS are different. For small voltage, the resistance changes a little while for large voltage, the resistance changes evident at the 1st cycle, as illustrated in Fig. 3.12. The decreasing output current with cycles is similar to the depression and habituation function of animals' synapse, suggesting that the memristor devices are potential to act as information storage cell and artificial synapse simultaneously. The synaptic plasticity should be explored with further study, like the implement of electric pulse, which is closer to bio-electricity signals.

3.4.3 Current-voltage characteristics of Au/Li-20PEO-SiO_2/Si

After adding the nano SiO_2 particle into the electrolyte membrane, the I-V properties change. Fig. 3.13 is the DC I-V curves of Au/Li-20PEO/Si and Au/Li-20PEO-SiO_2/Si. The curves are drawn in both logarithmic and linear coordinate. For curve in linear coordinates, it is processed symmetrically to gain a more intuitive observation of the curve symmetry. As illustrated in Fig. 3.13(c) and (d), with the cut-off voltage of ±5.0V, the resistance states of Au/Li-20PEO-SiO_2/Si have insignificant change with a resistance ratio smaller than 10. This may result from the lower ionic conductivity of Au/Li-20PEO-SiO_2/Si membrane. It shows certain stability as the RS tendency remain unchanged during sweeping.

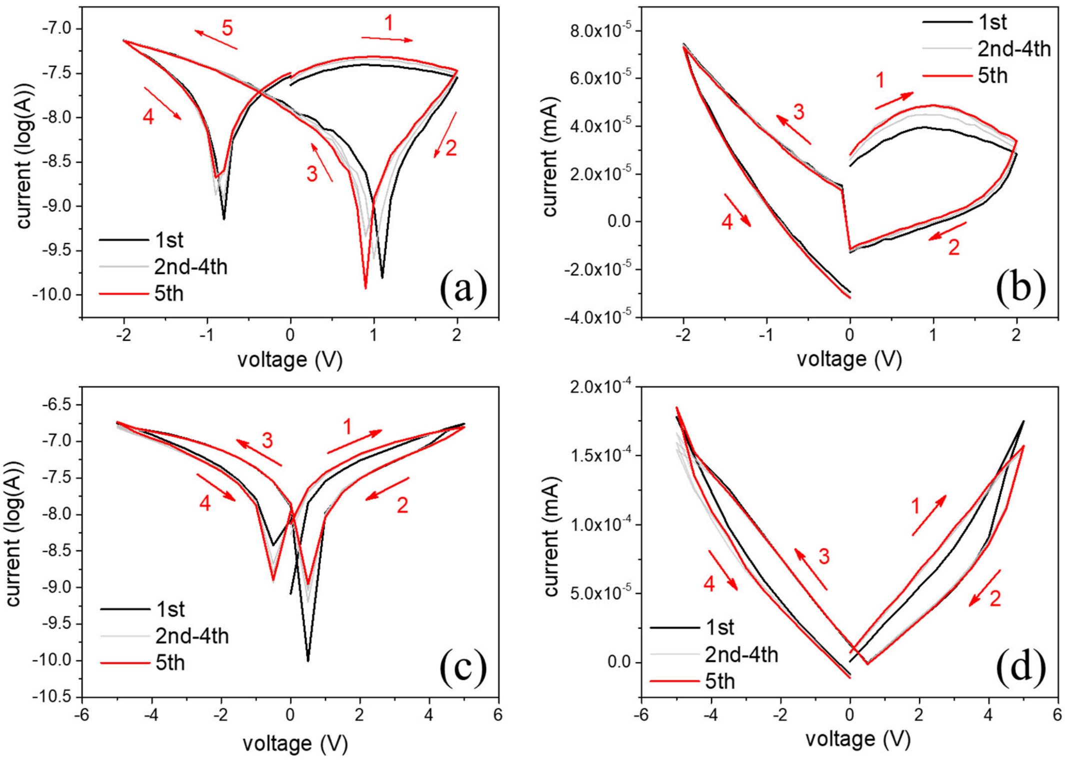

Fig. 3.13 DC current-voltage sweeping of Au/Li-20PEO/Si in (a)logarithmic coordinate and (b)linear coordinate and Au/Li-20PEO-SiO$_2$/Si in (c)logarithmic coordinate and (d)linear coordinate. The curves in linear coordinates are processed symmetrically

And compared to the Au/Li-20PEO/Si, the curve of Au/Li-20PEO-SiO2/Si is more symmetric under reverse bias, as demonstrated in Fig. 3.13. The symmetry can also be observed from Table 3.3, in which the current value is almost the same for Au/Li-20PEO-SiO$_2$/Si under both positive and negative bias. In some application fields, voltage amplitude is often used as a regulation index, which is independent of polarity. The symmetry property of Au/Li-20PEO-SiO$_2$/Si can be used in these fields.

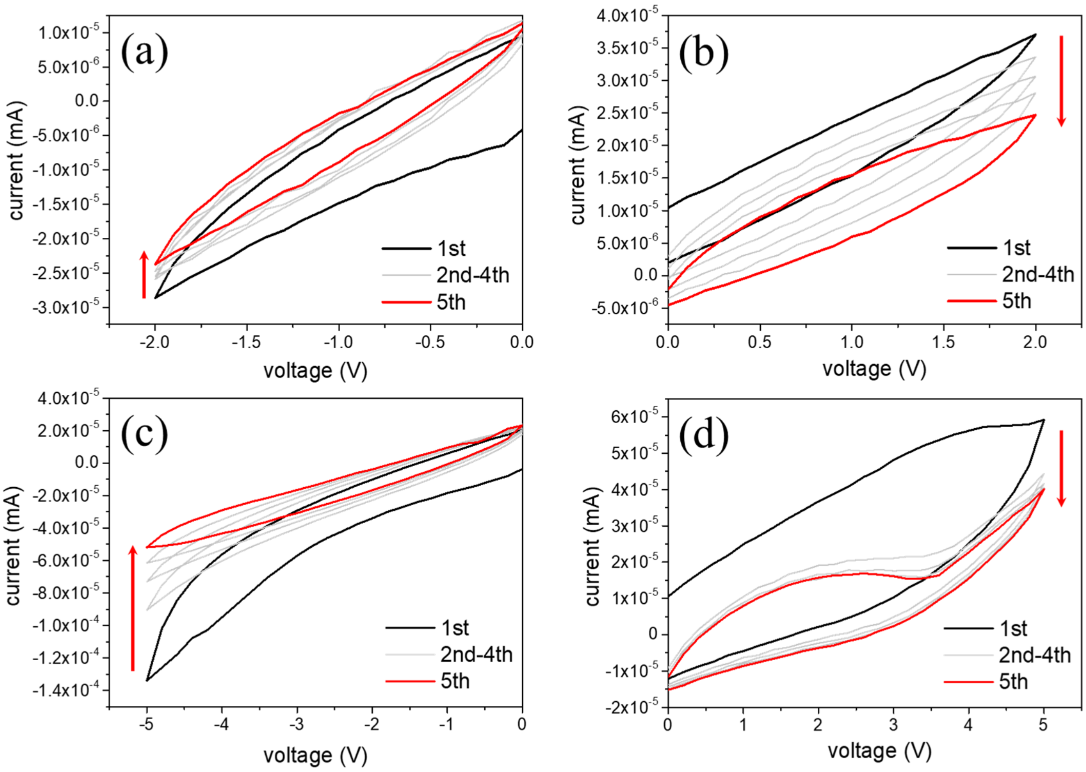

Fig. 3.14 Unipolar DC I-V sweeping of Au/Li-20PEO-SiO$_2$/Si. Negative bias from (a) 0 → -2.0V→ 0V and (c) 0 → -5.0V→ 0V. Positive bias from (b) 0 → 2.0V→ 0Vand (d) 0 → 5.0V→ 0V

The electric response under unipolar bias of Au/Li-20PEO-SiO$_2$/Si was illustrated in Fig. 3.14. The change of the current is the same as Au/Li-20PEO/Si, that is gradually decreasing with cycles regardless of the voltage polarity and shows multiple levels of resistance state. For small cut-off voltage, the hysteresis loop shows little change. For large cut-off voltage (±5.0V), the current drops off more between 1st and 2nd cycle compared to the following ones.

3.4.4 Working power consumption

From the discussion above, it can be seen that the minimum operating voltage for Au/Li-20PEO/Si and Au/Li-20PEO-SiO$_2$/Si memristor are both 5V, at which they show

SET behavior. The working power consumption were calculated by integrating the I-V curve[53], as listed in Table 3.4. For Au/Li-20PEO/Si, the power consumption is 0.495mW while for Au/Li-20PEO-SiO_2/Si, it is 0.413mW. With nano SiO_2 doped, the consumption is reduced by 16.57%, achieving the purpose of decreasing power consumption.

Table 3.4 Power consumption

Structure	Power consumption (mW)
Au/Li-20PEO/Si	0.495
Au/Li-20PEO-SiO_2/Si	0.413

3.5 Analysis of resistance switching mechanism

Based on the discussion above, the mechanism can be concluded below.

3.5.1 RS mechanism for Au/Li-20PEO/Si

Fig. 3.15 is the schematic of the RS process for Au/Li-20PEO/Si. Initially, the Li+ ions distribute uniformly as HRS in the electrolyte (Fig. 3.15a). When applying positive bias on the top electrode, Li+ ions move towards bottom electrode, which has a naturally grown oxide layer (SiO_2) on the surface (Fig. 3.15b). If the cut-off voltage is low (such as ±1V and ±2V in Fig. 3.11), the moved Li+ ions will diffuse backward spontaneously, then shows HRS under the following negative bias, as illustrated in Fig. 3.15(d) and (e). However, if the cut-off voltage is high (such as ±5V in Fig. 3.11), some of the Li^+ ions may be trapped in SiO_2 layer[2], which cannot diffuse backward spontaneously. The interaction of Li+ with SiO_2 can lead to lower resistance, showing SET behavior. With the following negative bias, these ions can be released then, showing RESET behavior, as discussed in section 3.4.

Under the consecutive unipolar bias in Fig. 3.12, the Li^+ cannot return or be released timely, causing less and less movable ions, thus demonstrating decreasing current. Under positive bias, Li^+ moves from top electrode towards bottom electrode within PEO layer while under negative bias, it moves from SiO_2 layer. Since the latter one needs more force than the former one, so the I-V properties exhibit asymmetrically under positive and negative bias.

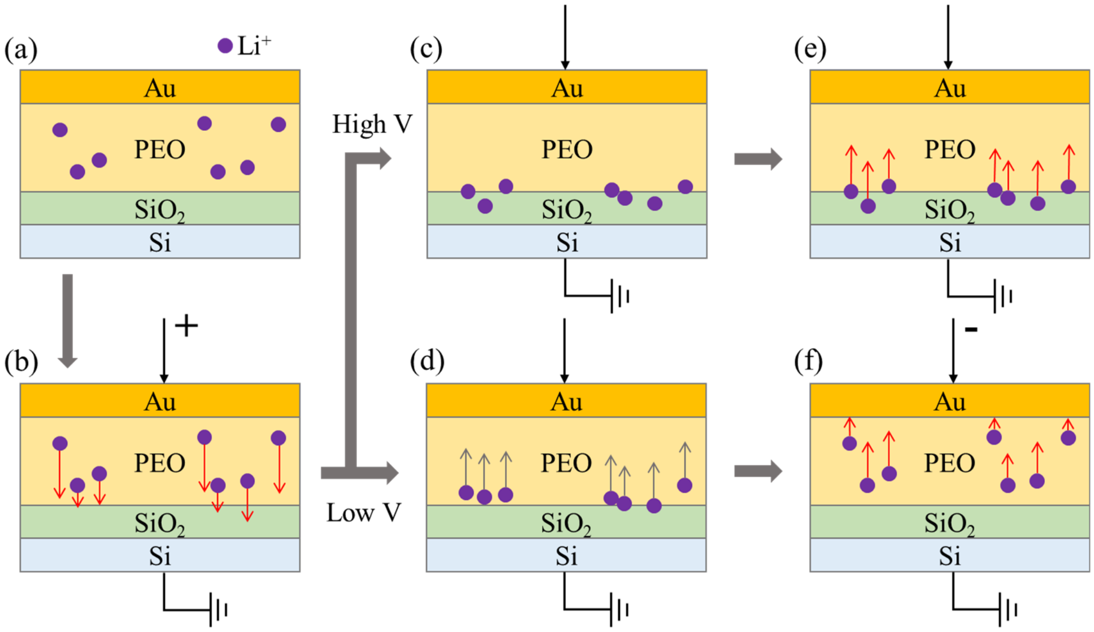

Fig. 3.15 Schematic of the RS process of Au/Li-20PEO/Si. (a) is the initial state, (b) is the condition under positive bias, (c) and (e) are the condition with high cut-off voltage while (d) and (f) are the condition with low cut-off voltage

3.5.2 RS mechanism for Au/Li-20PEO-SiO_2/Si

Fig. 3.15 is the schematic of the RS process for Au/Li-20PEO-SiO_2/Si. The electrolyte with Li^+ and nano SiO_2 particles dispersed is HRS initially (Fig. 3.16a). The Li^+ ions will move toward bottom electrode under applied positive bias but some ions are easy to be attracted near the nano SiO_2 particles as shown in EDS mapping in section 3.3.3, lowering the number of movable ions. So, the response current of Au/Li-20PEO-SiO_2/Si is smaller than Au/Li-20PEO/Si (Fig. 3.16b). Then with negative bias, the same process will occur, some ions be “trapped” by SiO_2 particles, some move after electric field. Since the SiO_2 are dispersed homogenously in PEO, so the I-V performance is symmetrically as demonstrated in Fig. 3.13.

Under consecutive unipolar bias in Fig. 3.14, more and more Li^+ ions are absorbed on the SiO_2 surface so the current decreases with the cycles, resulting in less and less migratable ions, as illustrated in Fig. 3.14.

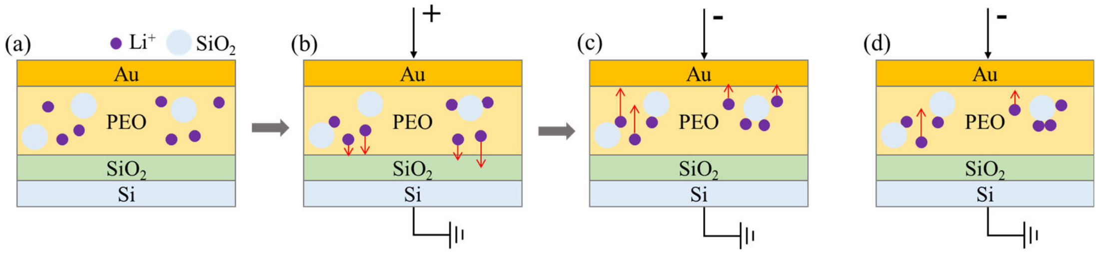

Fig. 3.16 Schematic of the RS process of Au/Li-20PEO-SiO_2/Si. (a) is the initial state, (b) is the condition under positive bias, (c) is the condition under negative bias. (d) is the condition after several cycles

3.6 Conclusion

In this chapter, we fabricated the Li-20PEO electrolyte used in Li ion based memristor and characterized the properties of the Au/Li-20PEO/Si and Au/Li-20PEO-SiO_2/Si devices. After doping the nano SiO_2 into the electrolyte layer, the working power consumption is decreased. The main conclusions include:

(1) The thickness can be improved by multi-step spin-coating method. Using multi-step spin-coating method instead of the traditional solution casting method, the thickness can be reduced from ~10μm to <100nm, which is of great importance to gain more compact hardware.

(2) The overall quality of the Li-20PEO electrolyte membrane is excellent. It has lower crystallinity with Li salt dispersed homogenously in PEO, confirmed by EDS mapping and XRD pattern. The thickness and roughness are also small enough, meeting the requirement for devices application. Meanwhile the membrane has certain ionic conductivity (1.78×10^{-5} S/cm, comparable to normal ionic conductivity).

(3) Au/Li-20PEO/Si shows both bipolar and memristive RS mode, suitable for digital and analog information storage respectively. Under appropriate conditions, the RS modes can convert to each other. The output current gradually increases and the hysteresis loop shrinks with unipolar consecutive bias, similar to the excitation and habituation of synapse. The RS mechanism of Au/Li-20PEO/Si is related to the ion movement and the spontaneous recover of the moved ions.

(4) Addition of nano SiO_2 into the electrolyte membrane can make the I-V properties of the devices more symmetric due to the uniformly dispersion of SiO_2. Improved symmetry of the devices broadens its application field. More importantly, doping with SiO_2 can decrease the working power consumption, which is reduced from 0.495mW to 0.413mW (16.57%).

Chapter 4 Preparation and Properties of Composite Li-ion based Memristor

4.1 Introduction

As discussed in chapter 3, addition of Li salt in the electrolyte function layer can realize the basic I-V properties (SET and RESET, certain ON/OFF ratio) of the memristor devices. Chapter 3 demonstrates that using lithium ions to achieve memristor function is realistic.

Ag is widely used as electrode in memristors due to its high activity. It's confirmed that for Ag electrode, it will form metallic filament from top side to bottom side as the conductive channel, known as conductive filaments (CFs). The diameter and stability of the conductive filaments can change with the external electrical stimulus, so that to realize the resistance switching. Banerjee et al. fabricated the hybrid Ag filament as the CFs in memristor devices[72] and achieve a better performance like extremely low OFF current, illuminating the recombination function of Ag and other elements. Another research has found that the Ag nanoparticles help to produce a strong interaction between the polymer and the free salt, interrupting crystallization process and increasing the content of amorphous phase[59].

Here, we try to combine the Li-PEO with Ag, aim to improve the properties of the Li-ion based memristor electrolyte, such as reducing the consumption, enhancing the stability and so on.

Before study the composition of Ag and Li, the single Ag based devices - Ag as the top electrode and pure PEO as the medium layer, were fabricated to confirm the conductive mechanism of Ag electrode. Then, the Ag/Li-20PEO/Si devices were fabricated. The electrical measurements, mainly the I-V sweeping cycles, were token to study the effect of synergistic effect of Ag CFs and Li ions on the resistance switching behaviors. After analyzing the I-V properties, the consumption was calculated and some mechanism mode was put forward.

4.2 Experiments

4.2.1 Fabrication of the PEO and Li-20PEO memristor

Ultrasonically cleaned the p-doped silicon substrate with acetone for 40 minutes, ethyl alcohol for 30 minutes and deionized water for 30 minutes. 0.08g PEO was dissolved in 5 mL acetonitrile in the glove box filled with Ar gas (water content < 0.01 ppm and O_2 content < 0.01 ppm). Then stirred the solution with magnetic stirring apparatus for 24h. The solution was then spin-coated on the substrate p-Si (or ITO substrate) in the glove box with multi-stepping spin-coating method, and cured at 40°C to 60°C for 2 hours. After curing, silver with thickness of ~120 nm was deposited on the PEO film by thermal evaporation through a shadow mask as the top electrode.

Preparation of the thicker Li-ion electrolyte membrane

4.2.2 Testing and characterization

DC I-V sweeping was used to characterize the electrical properties of the memristor devices with electrochemical workstation (4200A-SCS parameter analyzer) equipped with Probe Station. The DC I-V sweeping was conducted at ambient temperature and in the atmosphere. When analyzing the I-V property, the data in this chapter is all shown in single-logarithmic coordinate with absolute values.

Scanning Electron Microscope (SEM) was tested to measure the micro morphology of the pure PEO electrolyte membrane spin-coated on substrate ITO.

The working power consumption was calculated according to the equation (3-1).

4.3 Current -voltage characteristic analysis

4.3.1 Current-voltage characteristics of Ag/PEO/Si

The bias was applied on the top electrode while the bottom electrode was grounded. Even with a small bias (±1.0V in Fig. 4.1a), the device shows resistance switching (RS) behavior: the current suddenly increases at ~0.5V at positive bias and decreases at negative bias. The resistance switching behavior corresponds with the SET and RESET phenomena. With different cut-off voltage range (±1.0V, ±2.0V and ±5.0V), the RS behavior are all shown but unconspicuous at small bias range. Until the cut-off voltage increases to ±5.0V, a noticeable RS behavior appears. Therefore, ±5.0V was selected as the scanning cut-off voltage for 50 cycles, to observe the stability of the device. As Fig. 4.1(d) shows, though there is some difference between each cycle, the whole RS behavior is stable with the SET voltage ~3V but no distinct RESET voltage. For the 1st cycle, the SET behavior is unnoticeable with a small ON/OFF ratio (~100). From the 2nd cycle, the noticeable SET behavior occurs with a high ON/OFF ratio (~10^4), and the SET voltage keeps decreasing while cycling.

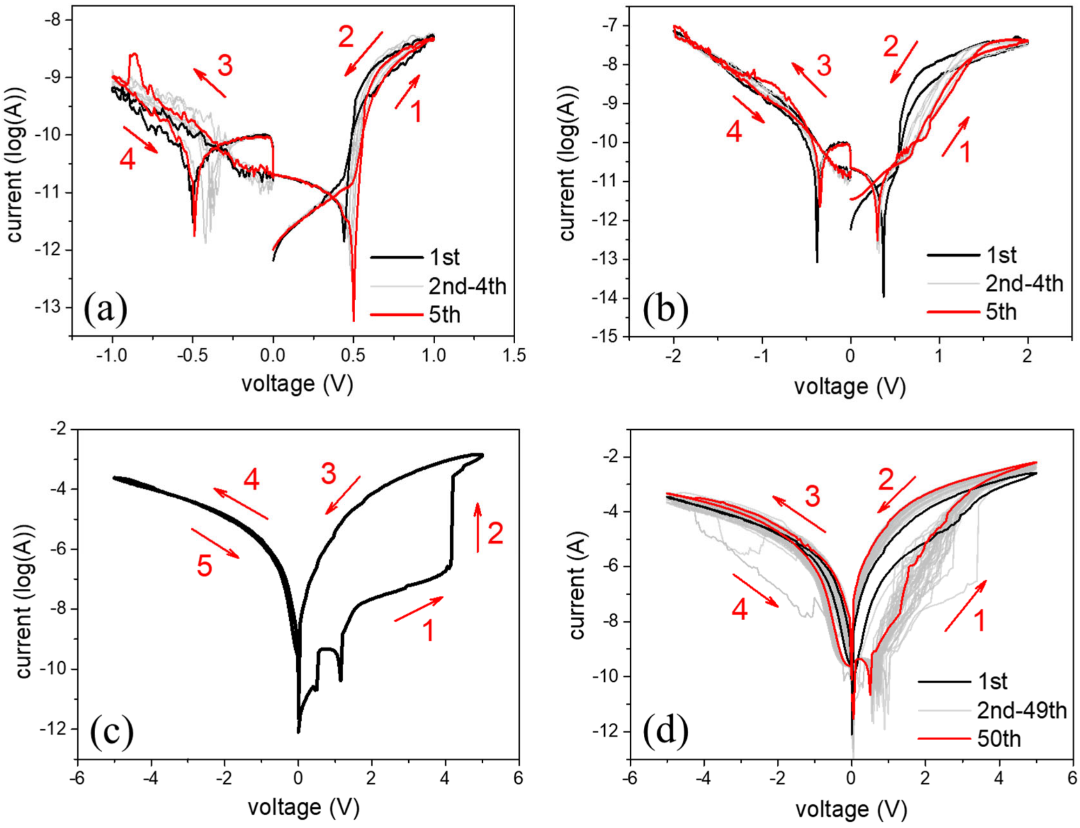

Fig. 4.1 DC current-voltage sweeping of Ag/PEO/Si. The cyclic sweeping started with a positive bias on top electrode. The sweeping range is (a) 0 → 1.0V → -1.0V→ 0V, (b) 0 → 2.0V → -2.0V→ 0V, (c) and (d) 0 → 5.0V → -5.0V→ 0V

This result indicates that the conductive Ag filament failed to penetrate the SiO_2 layer at the 1st lap. After the formation of Ag filament through the top electrode and the bottom electrode, it's easier for the next time to form conductive path, resulting in decreasing SET voltage. However, the filament within the SiO_2 layer is sensitive to the Joule heat and easy to thermal-fuse spontaneously, causing no RESET behavior to be observed.

In the I-V sweeping, the minimum current located at a non-zero voltage, which is related to the capacitive effect caused by the inhomogeneity of ions in the polymer[26]. Fluctuations of the switching voltage are one of the biggest obstacles in the application of resistance switches, due to the random formation and the varying degree of dissolution of conductive filaments in the dielectric layer[73].

4.3.2 Current-voltage characteristics of Ag/Li-20PEO/Si

The resistance switching properties of Ag/Li-20PEO/Si is demonstrated in Fig. 4.2. The cut-off voltage varies from ±1.0V to ±3.0V. With small cut-off voltage (±1.0V in Fig. 4.2a), both SET behavior occurs under both positive and negative bias strangely. With cut-off voltage of ±3.0V, the RS is stable with small deviation, as shown in Fig. 4.2(c). Therefore, ±3.0V was selected as the scanning cut-off voltage for 50 cycles. As shown in Fig. 4.2(d), each cycle overlaps with the others with high ON/OFF ratio ~10^5, representing the high stability and good RS property of the device.

Also, the voltage at which the current drops to zero are different under different cut-off voltages. For ±1.0V and ±2.0V, the current returns to zero even with nonzero voltage but for ±3.0V, the current becomes zero with voltage synchronously. The former one corresponds to threshold switching (TS) mode and the later one corresponds to memory switching (MS) mode[74]. In the MS mode, the resistance states can be maintained after the removing of the bias while in TS mode, the resistance state will be back to the initial one once the applied voltage is smaller than a critical value[75]. These two kinds switching mode can be interchangeable with proper conditions. In our case, with small voltage, the device shows volatile TS mode but with larger voltage, it shows MS mode. That is because the tiny stimulus causes only some weak CFs and after the removal of the bias, the CFs dissolve or fracture spontaneously and the device returns to initial states. But for larger voltage stimulus, it forms more amount and stronger CFs, which will rapture with the help of reverse external electric bias.

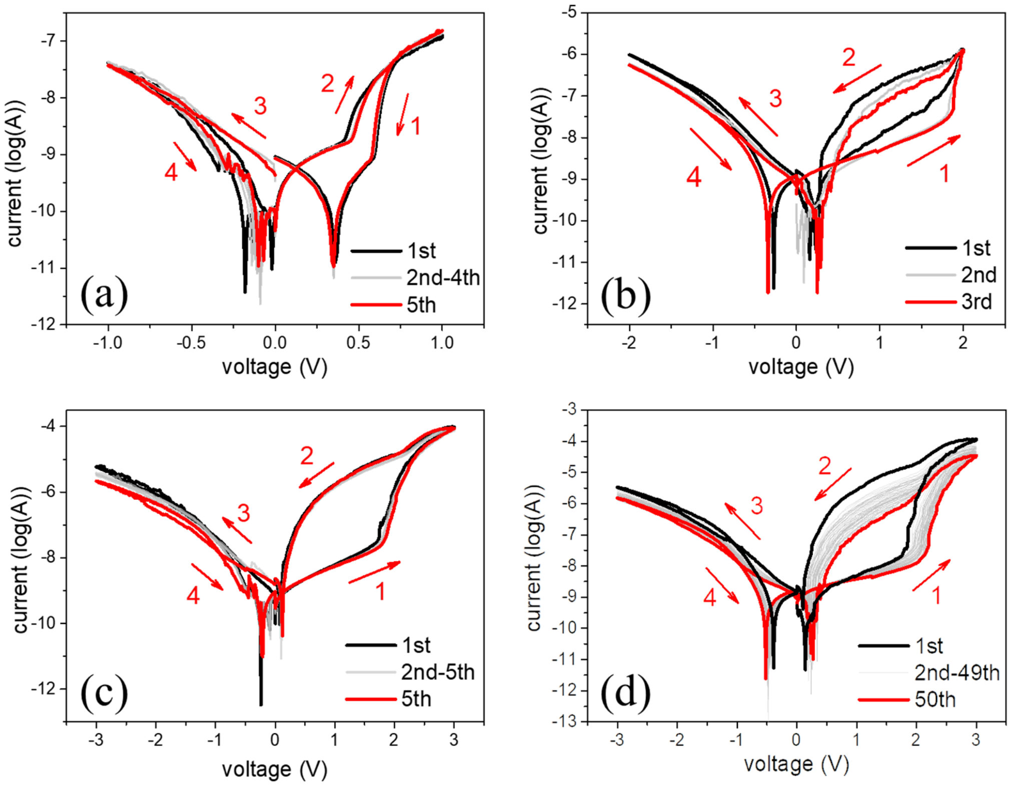

Fig. 4.2 DC current-voltage sweeping of Ag/Li-20PEO/Si. The sweeping range is (a) 0 → 1.0V → -1.0V→ 0V, (b) 0 → 2.0V → -2.0V→ 0V, (c) and (d) 0 → 3.0V → -3.0V→ 0V

With highly doped Li salt, the electrolyte membrane has large amorphous region initially, which is in favor of the Li ions transport and the formation of conductive filaments. But the Joule heat, especially during the RESET progress, will induce the recrystallization of the electrolyte materials, decreasing the ionic movement and conductivity. Therefore, when apply the negative bias, the devices degraded to high resistance state rapidly, showing little RESET.

To study the electric output under unipolar bias, applied consecutive unipolar bias on top electrode. As shown in Fig. 4.3(a), under unipolar negative bias, the first 4 cycles barely change. In this bias mode, Li ions move to top electrode and no conductive paths formed across the electrolyte layer, showing always HRS. There is a sudden enlarged current during 5th cycle, which may be related to increased conductivity from the heat-fused polymer region.

As shown in Fig. 4.3(b), it presents SET behavior under unipolar positive bias but the HRS shift upward and the ON/OFF ratio shrinks. That means under successive positive stimulus without negative stimulus, the conductive path form during the last cycle will remain, thus showing lower start-up resistance. Since for the CFs, the earliest formed filament will play a dominant role, and almost all the ions transfer through this filament. So, the LRS has a saturated state. In our case, the LRS reaches saturation at 2nd cycle. Therefore, the following cycles display nearly the same LRS value with 2nd and has decreased ON/OFF ratio. The increasing output current with cycles is similar to the excitation functions of synapse and the saturation is similar to the habituation function. It indicates the devices is available to mimic the functions of synapse and further the neutral network computation. The synaptic plasticity can be further explored with the implement of electric pulse, as mentioned in chapter 3.

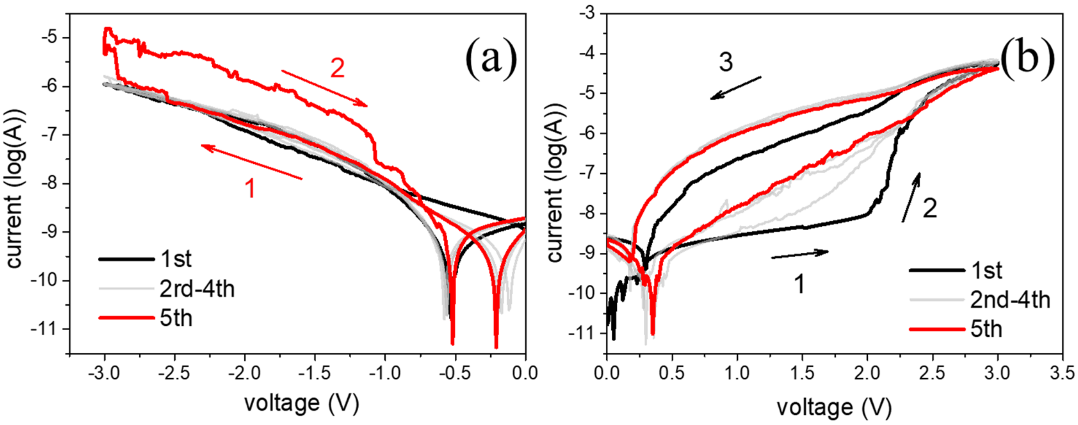

Fig. 4.3 Unipolar DC I-V sweeping of Ag/Li-20PEO/Si. (a) negative bias from 0 → -3.0V→ 0V. (b) positive bias from 0 → 3.0V→ 0V

Another noteworthy phenomenon is that for some specimen, the output current during I-V sweeping will increase or decrease a lot after leaving alone for a long time.

The increase may be caused by the diffusion of the extremely active Ag ions into the electrolyte layer and the decrease may be induced by the oxidation of electrode. In our experiment, some electrode points turned white after inputting continuous high voltage, which is also oxidize by the excessive heat released during test. It indicates that in practical application, some measures should be used to ensure the stability of the devices.

4.3.3 The influence of the naturally grown SiO_2 on I-V characteristics

As discussed above, there is no significant RESET behavior under negative bias and it may be caused by the influence of naturally grown SiO_2 layer on Si substrate. To exclude the influence of this oxide layer on the devices, fabricated Ag/PEO/ITO memristors. The indium tin oxide (ITO) is also widely used in memristors with its high conductivity. Using ITO instead of Si can help us clarify the mechanism of resistance changing. For the system with active metal as top electrode and PEO as the medium layer, some researches[27] have confirmed that the electrochemical metallization (ECM) is the leading mechanism, where the CFs will form and rapture according to the external electrical stimulus.

Fig. 4.4 is the SEM image of pure PEO membrane spin-coated on substrate ITO with magnification of 1,000× (Fig. 4.4a) and 4,000× (Fig. 4.4b). In Fig. 1(a), the grain boundary can be seen as the faint line. The wavy wrinkle in Fig. 1(b) may be caused by the destruction of high energy electron beam on the polymer. There are some particles in Fig. 4.4 (b), which may be the crystallization of PEO. The overall surface of PEO/ITO is homogeneous with little defects, indicating the flatness of the Ag/PEO/ITO devices. As for other system like Ag/PEO/Si and Ag/Li-20PEO/Si, the morphology was discussed in chapter 3. All of the membranes to assemble into devices has reliable uniformity.

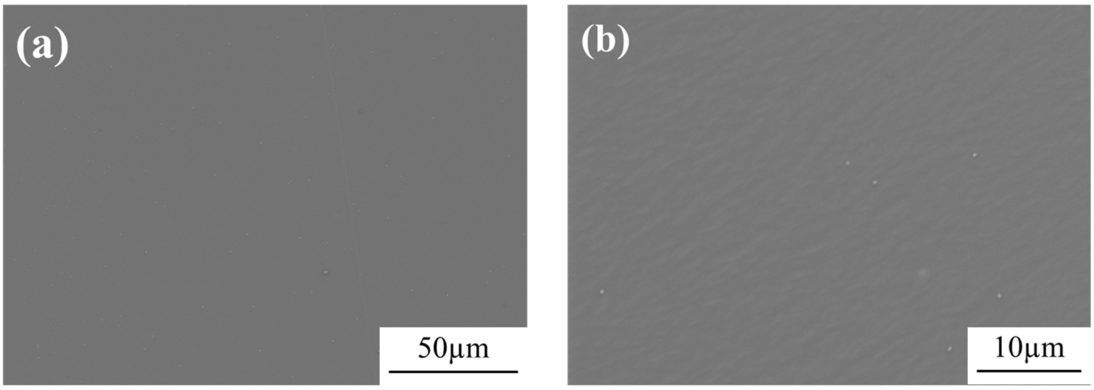

Fig. 4.4 SEM image of pure PEO spin-coated on substrate ITO. The magnification of (a) is 1,000× and that of (b) is 4,000×

As illustrated in Fig. 4.5, the SET appeared at positive bias and the RESET appeared at negative bias. At the first cycle (black line), it SET at ~2.5V with ON/OFF ratio ~10^7, corresponding to the forming process, and the device RESET at ~-2.8V. At the second cycle (red line), it SET at a lower voltage ~1.0V with lower ON/OFF ratio ~10^3, corresponding to the switching process. This is consistent with the literature, in which the SET and RESET are related to the formation and rapture of the conductive filaments respectively. During the 3rd to 5th cycles, the SET and RESET behaviors disappear, which may be the result of strong and steady CFs formed already, leading to continuous LRS, which is known as stuck-ON failure. The lower forming and switching voltage reveal that the natural growth SiO_2 on p-Si have passive impact on the RS properties, as discussed above.

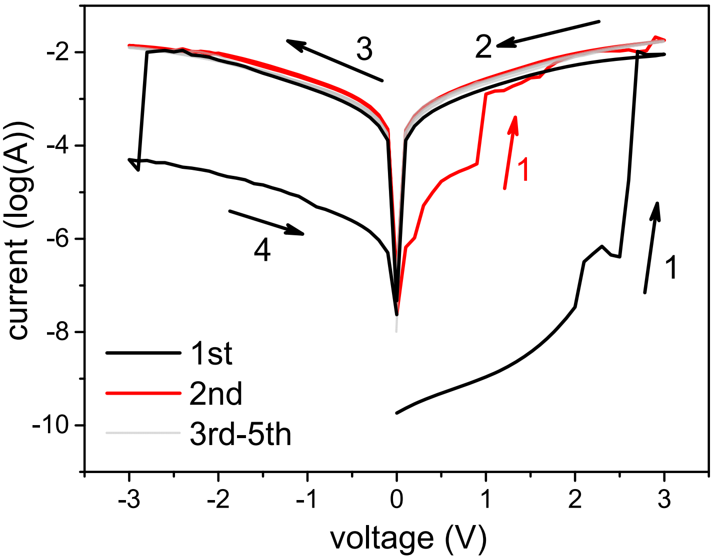

Fig. 4.5 DC current-voltage sweeping of Ag/ PEO/ITO with cut-off voltage of ±3.0V

Another factor that will influence the volatility is the Joule heat and the surface energy. Due to the influence of Joule heat and surface energy of active metallic particles, the filaments in the electrolyte layer gradually become nanoparticle[76, 77], leading the transformation of nonvolatility into volatility. Besides the recrystallization induced by Joule heat, excess Joule heat may even melt the polymer layer, causing an avalanche of ion migration, which is irreversible and devastating for the devices[78]. For some temperature sensitive materials, the accumulation of Joule heat may even lead to the decomposition of the polymer.

4.3.4 Working power consumption

From the discussion above, it can be seen that the minimum operating voltage for Ag/PEO/Si and Ag/Li-20PEO/Si memristor are 5V and 3V respectively, at which they firstly show SET behavior. The working power consumption were calculated by integrating the I-V curve, as listed in Table 4.1. For Ag/PEO/Si, the power consumption is 5.238mW while for Ag/Li-20PEO/Si, it is 1.128mW. Compared with Ag/PEO/Si, the consumption of Ag/Li-20PEO/Si is reduced by 78.47%, meaning that the Li ions in electrolyte layer can facilitate the RS behavior.

Table 4.1 Power consumption

Structure	Power consumption (mW)
Ag/PEO/Si	5.238
Ag/Li-20PEO/Si	1.128

4.4 Analysis of resistance changing mechanism

4.4.1 The resistance changing mechanism of Ag/ PEO/Si

For the Ag/PEO/Si structure, the active conductive ions are the Ag ions from the top electrodes. Once one Ag ions assemble and form one conductive filament (at which it reaches LRS), the subsequent ions will preferentially pass through this CF, making this CF stronger and stronger. If a higher external voltage is applied, other relatively weak CFs may be induced to form randomly. The weaker CFs are sensitive to the external stimulus and heat, easier to be broken. The fluctuation of the SET voltage around 2~4V (Fig. 4.2d) is related to the dissolution of some of the weak CFs.

As discussed above, the vague RESET behavior at negative bias is mainly caused by the thermal-fuse spontaneously and the recrystallization with the Joule heat, making the devices return to HRS even before the application of the reverse bias.

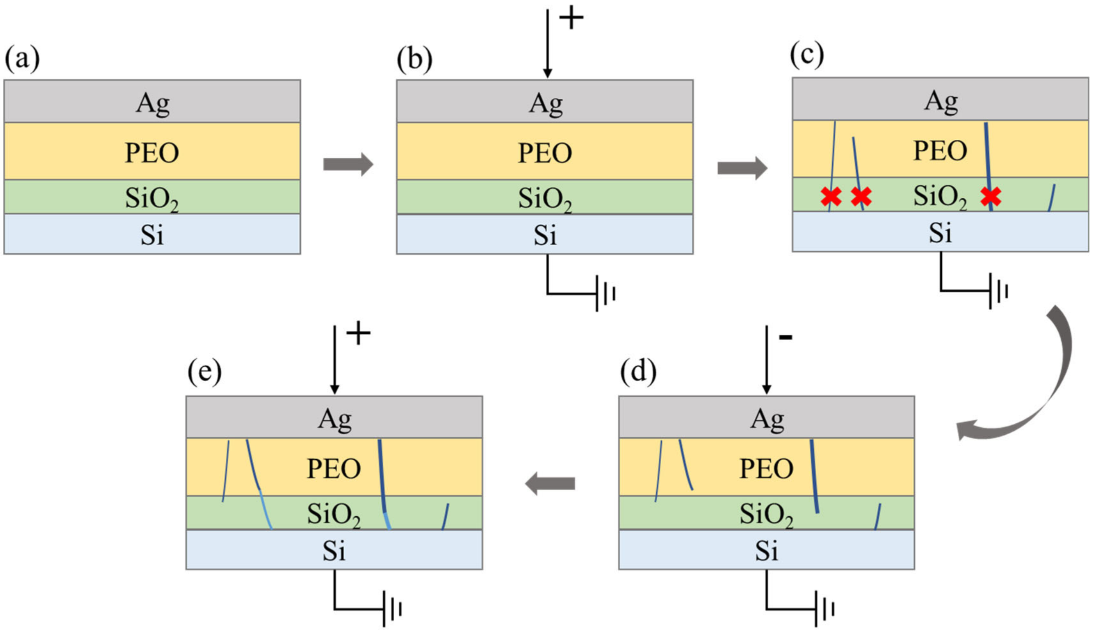

Fig. 4.6 Schematic of the RS process in Ag/PEO/Si. (a) is the initial state, (b) and (e) is the condition under positive bias, (c) is the condition with removal of the bias and (d) is the condition under negative bias. The stubs represent the CFs formed

Fig. 4.6 is the schematic of the RS process of Ag/PEO/Si with a layer of naturally grown SiO_2. It shows HRS initially (Fig. 4.6a). Same as Ag/PEO/ITO, Ag CFs form and penetrate the insulating SiO_2 layer, connecting the top electrode to bottom electrode under the positive bias. Thus, the devices transfer from the HRS to LRS (Fig. 4.6b). After removing the positive bias, the CFs within the SiO_2 layer are unstable, which are easy to thermal-fuse spontaneously (Fig. 4.6c). Therefore, when applying negative bias, the devices exhibit HRS with no obvious RESET can be observed (Fig. 4.6d). But no all the CFs disappear, so with the next positive bias, the Ag ions deposit on the remaining CFs preferentially (light blue stubs in Fig. 4.6e), making it easier to form conductive paths across the electrolyte layer.

4.4.2 The resistance changing mechanism of Ag/ Li-20PEO/Si

Compared with Fig. 4.1, the voltage at which the resistance switching reaches a stabilized state of Ag/Li-20PEO/Si (~3V) is smaller than that of Ag/PEO/Si (~5V). To distinguish if the RS mechanisms in Ag/PEO/Si and Ag/ Li-20PEO/Si are the same, applied a higher cut-off voltage (~5V) on Ag/Li-20PEO/Si, and the IV sweeping result is depicted in Fig. 4.7. Under positive bias, there are two RS stages at ~2V and ~4V for the 1st cycle. The ~2V one is stable for each cycle while the ~4V stage degraded to ~2.5V gradually.

The ~4V SET voltage corresponds to the formation of conductive Ag filament as the value consistent with the Ag/PEO/Si discussed in section 4.3. However, for Ag/PEO/Si, there is no noticeable SET at the 1st cycle but for Ag/Li-20PEO/Si, the ~4V SET appears even at the 1st cycle, representing that the conductive filaments are easier to be formed in this case. Easier-formation of conductive filaments indicates that the addition of Li salt is beneficial to the ion movement and the formation of conductive path through the medium layer.

As for the response of SET at ~2V, it can be interpreted as the transport of lithium ions. Li ion is inclined to be absorbed near the electrode and change the potential distribution in the electrode/electrolyte contact region, thus affecting the overall RS behavior. Consider the I-V properties of Au/Li-20PEO/Si in chapter 3, its resistance switching mechanism is mainly the migration of Li ions without the presence of active electrodes. The SET voltage of Au/Li-20PEO/Si is ~2V, matching the ~2V SET voltage here.

But the movement of Li ions is weak, which will be reduced spontaneously after the removal of external electrical field, showing volatility to some extent. This explains the unobvious RESET under negative bias. For Si substrate, there will be a layer of naturally grown SiO_2 naturally with thickness of about several nanometers. This insulating SiO_2 may also affect the electric performance of the device, such as accelerating the restoration of electrostatic effects of Li ions.

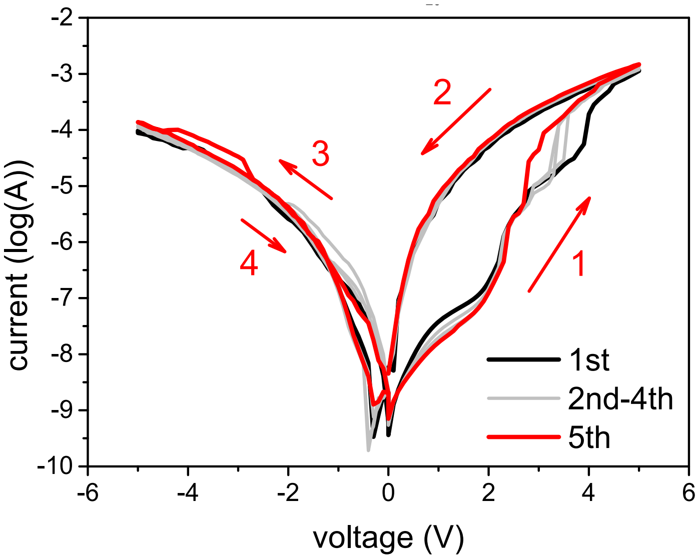

Fig. 4.7 DC current-voltage sweeping of Ag/Li-20PEO/Si with cut-off voltage of ±5.0V. The black line is the 1st cycle, the gray ones are the 2nd to 4th cycles and the red one is the 5th cycle. The arrows show the resistance changing direction

Fig. 4.8 is the schematic of the RS process of Ag/Li-20PEO/Si with naturally grown SiO_2. In initial state, the Li ions are distributed uniformly in PEO, exhibiting HRS (Fig. 4.8a). when applying the positive bias on the top electrode, the Li ions transfer towards bottom electrode and gathered at the electrolyte/electrode interface, changing the potential distribution there (Fig. 4.8b), which is the movement of Li ions, explaining the first SET at ~2V. during this process, some Ag ions also aggregate from the bottom electrode. The positive bias keeps larger, then the Ag ions finally eventually grow into CFs across the electrolyte membrane (Fig. 4.8c), corresponding to the second SET at ~4V and the LRS. After removing the bias, the CFs within SiO_2 layer is unstable and sensitive to the Joule heat. Therefore, the CFs thermal-fuse spontaneously, destroying the conductive channels (Fig. 4.8d). when the negative bias applies, the weak migration of Li ions is restored (Fig. 4.8e), leaving little RESET behavior. After one cycle, the devices return to its initial state HRS (Fig. 4.8f).

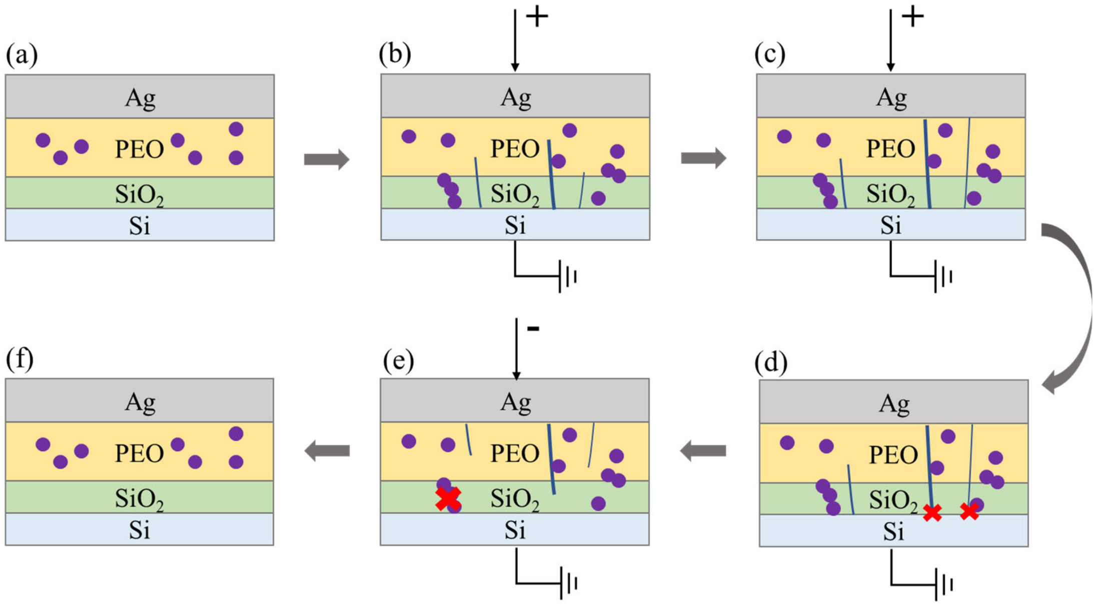

Fig. 4.8 Schematic of the RS process in Ag/Li-20PEO/Si. (a) is the initial state, (b) and (c) is the condition under positive bias, (d) is the condition after removing the positive bias, (e) is the condition under negative bias and (f) is the condition after removing negative bias. The stubs represent the CFs and the purple sphere represents the Li ions

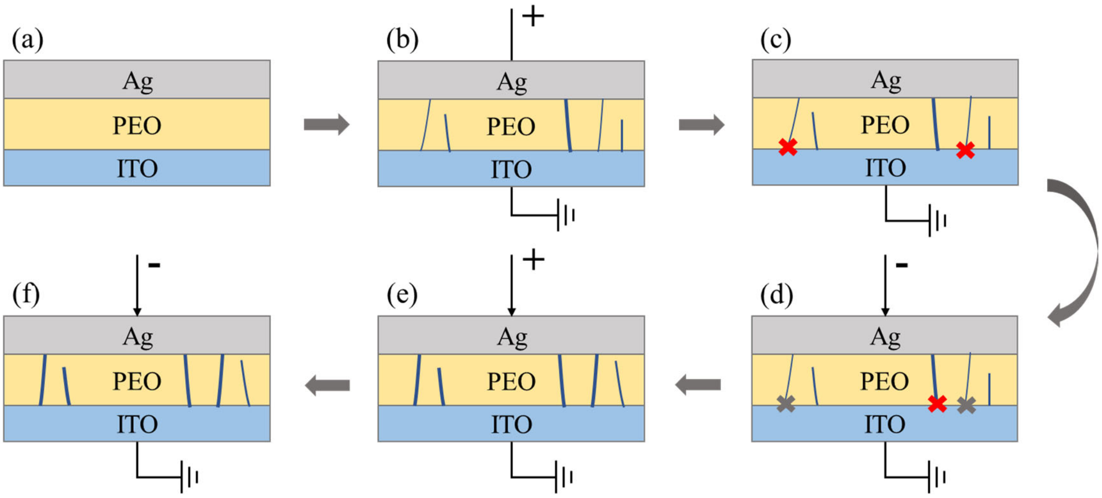

Fig. 4.9 Schematic of the RS process of Ag/PEO/ITO. (a) is the initial state, (b) and (e) are the condition under positive bias, (c) is the condition with removal of the bias and (d) and (f) are the condition under negative bias. The stubs represent the CFs formed

Fig. 4.9 is the schematic of the RS process of Ag/PEO/ITO. Initially, there is no CFs between the PEO electrolyte and the devices show HRS (Fig. 4.9a). When applying a positive bias, some Ag atoms dissolve from Ag electrode as Ag+ ions and move towards bottom electrode with the electric field. When the Ag+ ions contact the bottom electrode, they are reduced to be atoms and cluster at the PEO/ITO interface. With more and more atoms assemble, both robust and weak CFs will form (Fig. 4.9b), connecting the top and bottom electrodes, exhibiting LRS. After removing the bias, some weak CFs will break but the robust ones remain, displaying LRS still (Fig. 4.9c). Then when applying negative bias, the robust CFs will break as well with LRS return to HRS (Fig. 4.9d). But after several cycles, some strong CFs can be formed (Fig. 4.9e), which cannot be broken even with external negative bias, showing LRS all the time (Fig. 4.9f).

4.5 Conclusion

In this chapter, we fabricated the Ag/PEO/Si, Ag/Li-20PEO/Si, and Ag/PEO/ITO memristor devices. With different structure, the RS behaviors and RS mechanism are different. The SET and RESET voltage, power consumption and ON/OFF ratio of the devices with different structure were summarized in Table 4.2. Also, the minimum working voltage of different memristors are shown in Fig. 4.10. The main conclusions include:

(1) Compared with Au/Li-20PEO/Si, in which only the Li ions contributes to the RS, the stability of Ag/Li-20PEO/Si is better.

(2) When adding Li salt into electrolyte layer, Ag/Li-20PEO/Si memristor has lower power consumption (1.128mW) compared with Ag/PEO/Si (5.238mW), as well as decreased minimum working voltage. It represents the Li ions can facilitating the RS behavior and reduce the consumption (up to 78.47%). All the structures exhibit good ON/OFF ratio over 10^4, which is profitable for the information reading and recognition, especially for digital signal.

(3) Ag/Li-20PEO/Si have two distinguish conductance states, which can store more than 1 message at once, better than the devices with only one conductance state. The two states are caused by the ECM of Ag electrode and the migration of Li ions, respectively. For active electrode without Li ions in the electrolyte layer (Ag/PEO/ITO, Ag/PEO/Si), the ECM mechanism plays a leading role. The RS behaviors are caused by the formation and dissolvement of the active metallic CFs. For inert electrode with Li ions (Au/Li-20PEO-Si), no ECM and only the migration of Li ions works. To fabricate the devices with multi-levels of conductance state is a strategy to increase the data storage density.

(4) The naturally grown SiO_2 will influence the properties of devices. Consider the SET behavior, since there is a naturally grown SiO_2 as insulating layer on the Si, the SET voltage is higher than that of ITO. Also, the SiO_2 layer will influence the RESET behavior, as shown in Table 4.2 that the devices with Si as the substrate show little RESET behavior.

Table 4.2 I-V properties with different structure

Structure	SET voltage (V)	RESET voltage (V)	Power consumption (mW)	ON/OFF ratio
Ag/PEO/ITO	~2.5	~-2.8	/	~10^7
Ag/PEO/Si	~4	/	5.238	~10^4
Ag/Li-20PEO/Si	~2 & ~4	/	1.128	~10^4
Au/Li-20PEO/Si	~2	/	0.495	~10^5

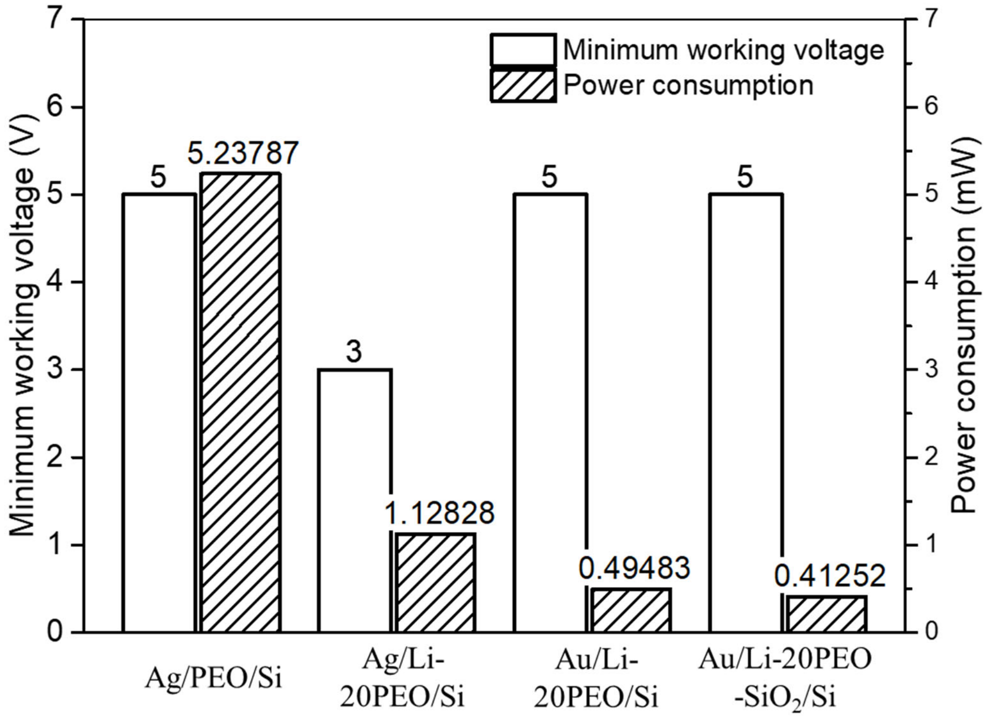

Fig. 4.10 Minimum working voltage and power consumption

In order to avoid the passive impact of the naturally grown SiO_2 on the Si, ITO or other substrates will be used as the substrate in subsequent experiments. Or we can deposit an inert metal layer between the Si and the medium electrolyte layer, to maintain the excellent compatibility of Si to CMOS circuits.

Chapter 5 Conclusion and Prospect

5.1 Conclusion

The ionic transport of memristor function layer material determines the comprehensive performance and practical application of ion based memristors. Inspired by the successful usage of LiTFSI-PEO complex in rechargeable battery, LiTFSI-PEO with certain ratio of EO and Li^+ was used to fabricate the Li-ion based memristor devices in our work to improve the working power consumption and RS behaviors.

The first two chapters focus on the background and development of memristors and the characterization procedures. The next two chapters are the fabrication and characterization of Li-ion based devices. The main work is summarized below:

(1) The Li-20PEO electrolyte membrane was fabricated with multi-step spin-coating method. With Li salt homogeneously doped in PEO, the crystallinity decreases and the membrane shows certain ionic conductivity. The thickness (<100nm) and roughness (<10nm) of the membrane can reach the requirement in practical application. Inert metal Au was used as top electrode and Au/Li-20PEO/Si was prepared. It shows both bipolar and memristive RS behaviors, which can be interpreted as the ion migration and spontaneous withdrawal.

(2) Nano SiO_2 particles with average diameter of ~10nm were added into the electrolyte and Au/Li-20PEO-SiO_2/Si memristor was fabricated. After the addition of SiO_2, the working power consumption is reduced from 0.495mW to 0.413mW (16.57%). Also, the response current in I-V sweeping decreases and has more symmetric I-V property.

(3) Active Ag electrode was used as top electrode (Ag/Li-20PEO/Si) to collaborate the effect of ECM and ion transfer. First the pure PEO as the electrolyte layer was used to study the formation and rapture of Ag CFs when applying external electrical stimulus. Then complexed Li salt into PEO to fabricate Ag/Li-20PEO/Si devices, which show stable SET and RESET RS behavior with large ON/OFF ratio of 10^5. With Li in electrolyte layer, the working voltage is decreased from 5V to 3V, and the power consumption is reduced from 5.238mW to 1.128mW (78.27%). Ag/Li-20PEO/Si memristor has two LRS, corresponding to Li ion migration and ECM of Ag respectively. Compared with ITO substrate, we can draw the conclusion that the naturally grown SiO_2 layer on Si will influence the electrical performance of the devices.

In conclusion, the Li-ion based memristor devices was fabricated with multi-step spin-coating method. The quality and electrical properties of Li-PEO membrane are comparable to those of general ones. The memristors show stable RS properties and the RS mechanism put forward can interpret the I-V behavior well. By doping nano SiO_2 into Li-PEO electrolyte or using active Ag as top electrode can both reduce the power consumption.

The application of LiTFSI-PEO adds a new choice to the fabrication of memristors, and it also provides new ways to reduce the consumption of memristor, which is useful for the research of ionic memristor in the future.

5.2 Shortcomings and prospect

In recent year, the explosive growth of artificial intelligence (AI) puts froward stricter demands for the storage density, calculation rate and so on, and memristor is the most promising candidate with various merits to usher in a new era of non-von Neumann computing. But there are still some challenges for the practical application of memristors like the stability. In our work, the instability and the working voltage of the devices should be further improved. And the RS mechanism should be confirmed by some characterization. The following concrete work can be carried out in the following aspects:

(1) Fabricate the devices with an inert metal layer deposited on Si or conductive glass like ITO as the bottom electrode, to exclude the passive impact of naturally grown SiO_2 on the electrical properties. Deposition of inert metal on Si can maintain the excellent compatibility of Si to CMOS circuits.

(2) Dissolve the nano SiO_2 particles better in Li-PEO to incorporate the advantages of nano fillers and the Li ions. Some method includes adding silane coupling agent into the electrolyte membrane.

(3) More characterization like the in-situ observation, planar observation and XPS should be conducted to demonstrate the element distribution after SET, further to confirm the RS mechanism.

(4) Use other type of electrical stimulation like pulses to simulate the synaptic plasticity. In our current work, the synaptic plasticity is preliminarily studied by the unipolar consecutive voltage, which is far from real conditions. The implement of pulse is closer to bio-electricity signals. The next work is to realize synaptic plasticity of the memristor.

REFERENCE

[1] IELMINI D. Brain-inspired computing with resistive switching memory (RRAM): Devices, synapses and neural networks [J]. Microelectronic Engineering, 2018, 190(1): 44-53.

[2] IOANNOU P S, KYRIAKIDES E, SCHNEEGANS O, et al. Evidence of Biorealistic Synaptic Behavior in Diffusive Li-based Two-terminal Resistive Switching Devices [J]. Sci Rep, 2020, 10(1): 8711-20.

[3] ZHANG C, CHEN Y, YI M, et al. Recent progress in memristors for stimulating synaptic plasticity [J]. SCIENTIA SINICA Informationis, 2018, 48(2): 115-42.

[4] LEE C, LEE J, KIM M, et al. Two-Terminal Structured Synaptic Device Using Ionic Electrochemical Reaction Mechanism for Neuromorphic System [J]. IEEE Electron Device Letters, 2019, 40(4): 546-9.

[5] FULLER E J, GABALY F E, LEONARD F, et al. Li-Ion Synaptic Transistor for Low Power Analog Computing [J]. Adv Mater, 2017, 29(4): 1604310.

[6] KUZUM D, JEYASINGH R G D, LEE B, et al. Nanoelectronic Programmable Synapses Based on Phase Change Materials for Brain-Inspired Computing [J]. Nano Letters, 2012, 12(5): 2179-86.

[7] SHARBATI M T, DU Y, TORRES J, et al. Low-Power, Electrochemically Tunable Graphene Synapses for Neuromorphic Computing [J]. Advanced Materials, 2018, 30(1802353.

[8] MAI V H, MORADPOUR A, SENZIER P A, et al. Memristive and neuromorphic behavior in a LixCoO2 nanobattery [J]. Scientific Reports, 2015, 5(1): 7761.

[9] CHUA. memristor-the missing circuit element [J]. IEEE Transactions Circuit theory, 1971, 18(5): 507-19.

[10] STRUKOV D B, SNIDER G S, STEWART D R, et al. The missing memristor found [J]. Nature, 2008, 453(7191): 80-3.

[11] GAO S, YI X, SHANG J, et al. Organic and hybrid resistive switching materials and devices [J]. Chemical Society Reviews, 2019, 48(6): 1531-65.

[12] 封扬. 基于溶液法的有机忆阻器及其神经元突触模拟研究 [D]; 苏州大学, 2019.

[13] WU C, LI X, XU X, et al. Self-rectifying resistance switching memory based on a dynamic p-n junction [J]. Nanotechnology, 2021, 32(8): 085203.

[14] YAN X, LI X, ZHOU Z, et al. Flexible Transparent Organic Artificial Synapse Based on the Tungsten/Egg Albumen/Indium Tin Oxide/Polyethylene Terephthalate Memristor [J]. ACS Applied Materials & Interfaces, 2019, 11(20): 18654-61.

[15] WU C, KIM T W, GUO T, et al. Mimicking Classical Conditioning Based on a Single Flexible Memristor [J]. Adv Mater, 2017, 29(10): 1602890.

[16] VU Q A, KIM H, NGUYEN V L, et al. A High-On/Off-Ratio Floating-Gate Memristor Array on a Flexible Substrate via CVD-Grown Large-Area 2D Layer Stacking [J]. Adv Mater, 2017, 29(44): 1703363.

[17] LIU C, CAO Y-Q, WU D, et al. Simulation of Biologic Synapse Through Organic-Inorganic Hybrid Memristors Using Novel Ti-Based Maleic Acid/TiO2 Ultrathin Films [J]. IEEE Electron Device Letters, 2020, 41(1): 155-8.

[18] FENG X, LI Y, WANG L, et al. A Fully Printed Flexible MoS2 Memristive Artificial Synapse with Femtojoule Switching Energy [J]. Advanced Electronic Materials, 2019, 5(12): 1900740.

[19] QIAN K, TAY R Y, NGUYEN V C, et al. Hexagonal Boron Nitride Thin Film for Flexible Resistive Memory Applications [J]. Advanced Functional Materials, 2016, 26(13): 2176-84.

[20] YALAGALA B, KHANDELWAL S, J D, et al. Wirelessly destructible MgO-PVP-Graphene composite based flexible transient memristor for security applications [J]. Materials Science in Semiconductor Processing, 2019, 104(104673.

[21] XIONG W, ZHU L, YE C, et al. Flexible Poly(Vinyl Alcohol)-Graphene Oxide Hybrid Nanocomposite Based Cognitive Memristor with Pavlovian-Conditioned Reflex Activities [J]. Advanced Electronic Materials, 2020, 6(1): 1901402.

[22] XU W, MIN S-Y, HWANG H, et al. Organic core-sheath nanowire artificial synapses with femtojoule energy consumption [J]. Science Advances, 2016, 2(6): e1501326.

[23] MCFARLANE T, BANDERA Y, GRANT B, et al. Carbazole Derivatized n-Alkyl Methacrylate Polymeric Memristors as Flexible Synaptic Substitutes [J]. Advanced Electronic Materials, 2020, 6(6): 200042-9.

[24] MA C, LUO Z, HUANG W, et al. Sub-nanosecond memristor based on ferroelectric tunnel junction [J]. Nature Communications, 2020, 11(1): 1439.

[25] LIU D-Q, CHENG H-F, ZHU X, et al. Research progress of memristors and memristive mechanism [J]. Acta Physica Sinica, 2014, 63(18): 187301.

[26] KRISHNAN K, TSURUOKA T, MANNEQUIN C, et al. Mechanism for Conducting Filament Growth in Self-Assembled Polymer Thin Films for Redox-Based Atomic Switches [J]. Adv Mater, 2016, 28(4): 640-8.

[27] VALOV I, WASER R, JAMESON J R, et al. Electrochemical metallization memories—fundamentals, applications, prospects [J]. Nanotechnology, 2011, 22(25): 254003-24.

[28] GE J, ZHANG S, LIU Z, et al. Flexible artificial nociceptor using a biopolymer-based forming-free memristor [J]. Nanoscale, 2019, 11(14): 6591-601.

[29] 徐航宇. 金属锂聚合物电池关键材料研究 [D]; 中国科学院大学(中国科学院物理研究所), 2019.

[30] FENTON D E, PARKER J M, WRIGHT P. Complexes of alkali metal ions with poly(ethylene oxide) [J]. Polymer, 1973, 14(589): 589.

[31] FARRINGTON G C, BRIANT J L. Fast Ionic Transport in Solids [J]. Science,

1979, 204(4400): 1371-9.

[32] GUILHERME L A, BORGES R S, MORAES E M S, et al. Ionic conductivity in polyethylene-b-poly(ethylene oxide)/lithium perchlorate solid polymer electrolytes [J]. Electrochimica Acta, 2007, 53(4): 1503-11.

[33] ZAN W, ZHANG Q, XU H, et al. Large capacitance and fast polarization response of thin electrolyte dielectrics by spin coating for two-dimensional MoS2 devices [J]. Nano Research, 2018, 11(7): 3739-45.

[34] XUE Z, HE D, XIE X. Poly(ethylene oxide)-based electrolytes for lithium-ion batteries [J]. Journal of Materials Chemistry A, 2015, 3(38): 19218-53.

[35] 李雪. PEO 基聚合物电解质及其锂硫电池性能研究 [J]. 电化学, 2020, 26(3): 338-46.

[36] ZHANG H, LIU C, ZHENG L, et al. Lithium bis(fluorosulfonyl)imide/poly(ethylene oxide) polymer electrolyte [J]. Electrochimica Acta, 2014, 133(1): 529-38.

[37] MARZANTOWICZ M, DYGAS J R, KROK F, et al. Phase segregation phenomena in poly(ethylene oxide):LiN(CF3SO2)2 electrolyte studied by local Raman spectroscopy [J]. Electrochimica Acta, 2010, 55(19): 5446-52.

[38] OGUZ O, SIMSEK E, KOSAK SOZ C, et al. Effect of filler content on the structure-property behavior of poly(ethylene oxide) based polyurethaneurea-silica nanocomposites [J]. Polymer Engineering & Science, 2018, 58(7): 1097-107.

[39] 李雪. PEO 基聚合物电解质的制备及全固态锂硫电池性能研究 [D]; 厦门大学, 2019.

[40] YANG T, ZHENG J, CHENG Q, et al. Composite Polymer Electrolytes with Li7La3Zr2O12 Garnet-Type Nanowires as Ceramic Fillers: Mechanism of Conductivity Enhancement and Role of Doping and Morphology [J]. ACS Appl Mater Interfaces, 2017, 9(26): 21773-80.

[41] TAN X, WU Y, TANG W, et al. Preparation of Nanocomposite Polymer Electrolyte via In Situ Synthesis of SiO2 Nanoparticles in PEO [J]. Nanomaterials (Basel), 2020, 10(1): 157-68.

[42] LI X, YANG L, SHAO D, et al. Preparation and application of poly(ethylene oxide)-based all solid-state electrolyte with a walnut-like SiO_2 as nano-fillers [J]. Journal of Applied Polymer Science, 2019, 137(24): 48810.

[43] FAN L, NAN C-W, ZHAO S. Effect of modified SiO2 on the properties of PEO-based polymer electrolytes [J]. Solid State Ionics, 2003, 164(1): 81-6.

[44] LEE E, HONG J-Y, UNGAR G, et al. Crystallization of poly(ethylene oxide) embedded with surface-modified SiO2 nanoparticles [J]. Polymer International, 2013, 62(7): 1112-22.

[45] SHEN X, LI R, MA H, et al. Enhancing Li+ transport kinetics of PEO-based polymer electrolyte with mesoporous silica-derived fillers for lithium-ion batteries [J]. Solid State Ionics, 2020, 354(115412.

[46] LI X, YANG L, SHAO D, et al. Preparation and application of poly(ethylene

oxide)-based all solid-state electrolyte with a walnut-like SiO2 as nano-fillers [J]. Journal of Applied Polymer Science, 2020, 137(24): 48810.

[47] ZHU Y, GONZALEZ-ROSILLO J C, BALAISH M, et al. Lithium-film ceramics for solid-state lithionic devices [J]. Nature Reviews Materials, 2020, 6(313–31.

[48] WANG S, WANG W, YAKOPCIC C, et al. Experimental study of LiNbO3 memristors for use in neuromorphic computing [J]. Microelectronic Engineering, 2017, 168(37-40.

[49] SHU W, WANG W, YAKOPCIC C, et al. Lithium based memristive device; proceedings of the Aerospace & Electronics Conference, F, 2016 [C].

[50] GREENLEE J D, PETERSBURG C F, CALLEY W L, et al. In-situ oxygen x-ray absorption spectroscopy investigation of the resistance modulation mechanism in LiNbO2 memristors [J]. Applied Physics Letters, 2012, 100(18): 182106.

[51] WEI H, YU H, GONG J, et al. Lithium Ion Alloying-Type Artificial Synapses [J]. ACS Applied Electronic Materials, 2019, 2(2): 316-22.

[52] ZHAO X, LI Y, AI C, et al. Resistive Switching Characteristics of Li-Doped ZnO Thin Films Based on Magnetron Sputtering [J]. Materials, 2019, 12(8): 1282.

[53] SHARBATI M T, DU Y, TORRES J, et al. Low-Power, Electrochemically Tunable Graphene Synapses for Neuromorphic Computing [J]. Adv Mater, 2018, 30(1): 1802353.

[54] LI J, JIANG D, YANG Y, et al. Li-Ion Doping as a Strategy to Modulate the Electrical-Double-Layer for Improved Memory and Learning Behavior of Synapse Transistor Based on Fully Aqueous-Solution-Processed In_2O_3 / AlLiO Film [J]. Advanced Electronic Materials, 2020, 6(4): 1901363.

[55] DUAN W. Room-temperature fabricated artificial synapse modulated by ultrathin SiO buffer layer [J]. Materials Letters, 2020, 261(127093-6.

[56] CHEN J, LIN C-Y, LI Y, et al. LiSiOX-Based Analog Memristive Synapse for Neuromorphic Computing [J]. IEEE Electron Device Letters, 2019, 40(4): 542-5.

[57] CHOI Y, LEE C, KIM M, et al. Structural Engineering of Li-Based Electronic Synapse for High Reliability [J]. IEEE Electron Device Letters, 2019, 40(12): 1992-5.

[58] WU Z, LU J, SHI T, et al. A Habituation Sensory Nervous System with Memristors [J]. Advanced Materials, 2020, 32(46): 2004398.

[59] MORSI M A, EL-KHODARY S A, RAJEH A. Enhancement of the optical, thermal and electrical properties of PEO/PAM:Li polymer electrolyte films doped with Ag nanoparticles [J]. Physica B: Condensed Matter, 2018, 539(88-96.

[60] CHEN S, LOU Z, CHEN D, et al. An Artificial Flexible Visual Memory System Based on an UV-Motivated Memristor [J]. Adv Mater, 2018, 30(7): 1705400.

[61] LIU Y, HU Y, ZHANG X, et al. Inhibited aggregation of lithium salt in spiro-OMeTAD toward highly efficient perovskite solar cells [J]. Nano Energy, 2020, 70(104483.

[62] ASMATULU R, KHAN W S. Chapter 13 - Characterization of electrospun

nanofibers [M]//ASMATULU R, KHAN W S. Synthesis and Applications of Electrospun Nanofibers. Elsevier. 2019: 257-81.

[63] 刘桂良，何宗倍，王梓璇, et al. CVD 沉积工艺对 SiC 涂层结晶度与耐腐蚀性能的影响 [J]. 复合材料科学与工程, 2021, 03): 71-7.

[64] 雷彤，赵孔双. 导电高分子膜的电化学阻抗谱研究进展 [J]. 化学通报, 2001, 01): 11-7.

[65] ZHAO Y, WU C, PENG G, et al. A new solid polymer electrolyte incorporating Li10GeP2S12 into a polyethylene oxide matrix for all-solid-state lithium batteries [J]. Journal of Power Sources, 2016, 301(47-53.

[66] FENG J, WANG L, CHEN Y, et al. PEO based polymer-ceramic hybrid solid electrolytes: a review [J]. Nano Converg, 2021, 8(1): 2.

[67] BORGHINI M C, MASTRAGOSTINO M, PASSERINI S, et al. Electrochemical Properties of Polyethylene Oxide - Li[(CF3SO2)2N] - Gamma - LiAlO2 Composite Polymer Electrolytes [J]. Journal of The Electrochemical Society, 1995, 142(7): 2118-21.

[68] AZLI A A, MANAN N S A, KADIR M F Z. Conductivity and Dielectric Studies of Lithium Trifluoromethanesulfonate Doped Polyethylene Oxide-Graphene Oxide Blend Based Electrolytes [J]. Advances in Materials Science and Engineering, 2015, 2015(145735.

[69] GUPTA H, SHALU, BALO L, et al. Effect of phosphonium based ionic liquid on structural, electrochemical and thermal behaviour of polymer poly(ethylene oxide) containing salt lithium bis(trifluoromethylsulfonyl)imide [J]. RSC Advances, 2016, 6(91): 87878-87.

[70] 屠芳芳，谢健，郭锋, et al. 基于 Li6.4La3Zr1.4Ta0.6O12 聚合物复合固态电解质的制备及电化学性能 [J]. 无机化学学报, 2020, 36(8): 1515-23.

[71] LIU Y, LEE J Y, HONG L. In situ preparation of poly(ethylene oxide)–SiO2 composite polymer electrolytes [J]. Journal of Power Sources, 2004, 129(2): 303-11.

[72] BANERJEE W, KARPOV I V, AGRAWAL A, et al. Highly-stable (< 3% fluctuation) Ag-based Threshold Switch with Extreme-low OFF Current of 0.1 pA, Extreme-high Selectivity of 109 and High Endurance of 109 Cycles; proceedings of the 2020 IEEE International Electron Devices Meeting (IEDM), F 12-18 Dec. 2020, 2020 [C].

[73] TSAI T L, JIANG F S, HO C H, et al. Enhanced Properties in Conductive-Bridge Resistive Switching Memory With Oxide-Nitride Bilayer Structure [J]. IEEE Electron Device Letters, 2016, 37(10): 1284-7.

[74] LI H-Y, HUANG X-D, YUAN J-H, et al. Controlled Memory and Threshold Switching Behaviors in a Heterogeneous Memristor for Neuromorphic Computing [J]. Advanced Electronic Materials, 2020, 6(8): 2000309.

[75] SUN H, LIU Q, LI C, et al. Direct Observation of Conversion Between Threshold Switching and Memory Switching Induced by Conductive Filament Morphology

[J]. Advanced Functional Materials, 2014, 24(36): 5679-86.

[76] WANG Z, JOSHI S, SAVEL'EV S E, et al. Memristors with diffusive dynamics as synaptic emulators for neuromorphic computing [J]. Nature Materials, 2017, 16(1): 101-8.

[77] YANG Y, GAO P, LI L, et al. Electrochemical dynamics of nanoscale metallic inclusions in dielectrics [J]. Nat Commun, 2014, 5(1): 4232-40.

[78] 杨慧永. 聚合物基忆阻器的性能研究及机制分析 [D]; 兰州大学, 2020.

Acknowledgements

In School of Materials Science and Engineering of SJTU, I spent my wonderful and colorful undergraduate career. At first, I would like to thank my supervisor Assi. Prof. Wu Yunwen, for her guidance, patience and encouragement. She provided me many technical supports, advice and helped me a lot. Also, I would like to thank my senior schoolmates, Zhang Jiani, Yao Yiyuan, Hu Wang and Tian Yuan. They taught and guided me through every single step of my work and gave me many useful suggestions. I also have many good friends around me, we studied together, we struggled together. In my study and life, I get a lot of help from them. So, I would like to thank all of the friends who helped me and encouraged me. And I want to express my appreciation to my family, for their supporting and their love.